# FEASIBILITY STUDY OF A PROTOTYPE MINIATURIZED METABOLIC GAS ANALYSIS SYSTEM FOR MAXIMAL EXERCISE TESTING

by

Tamara Lynn Anderson

A thesis submitted to the faculty of
The University of Utah
in partial fulfillment of the requirements for the degree of

Master of Science

Department of Bioengineering

The University of Utah

December 2010

**The University of Utah Graduate School**

# STATEMENT OF THESIS APPROVAL

The thesis of **Tamara Lynn Anderson**

has been approved by the following supervisory committee members:

| | | |
|---|---|---|
| **Dwayne Westenskow** | , Chair | **10/25/2010** Date Approved |
| **Joseph Orr** | , Member | **10/14/2010** Date Approved |
| **Rob MacLeod** | , Member | **10/25/2010** Date Approved |

and by **Richard D. Rabbitt** , Chair of the Department of **Bioengineering**

and by Charles A. Wight, Dean of The Graduate School.

# ABSTRACT

Metabolic gas analysis systems are important devices that are used to analyze respiratory gas exchange including volumetric flow rates and oxygen and carbon dioxide concentrations. This information provides useful insights into metabolic function. Traditionally, these systems were limited by their size and the functional requirements of the gas sensors including its sensitivity to water vapor and the alignment of flow and gas signals for real time analysis. Recently, Phillips-Respironics has developed a novel oxygen sensor that utilizes luminescence technology for oxygen analysis. When combined with a differential-pressure transducer and an on-airway nondispersive infrared $CO_2$ sensor, the result is a compact system suitable for real time breath-by-breath gas analysis. The system has been validated for use in a critical care environment with low respiratory flows of ±180 L/min. The purpose of this study was to determine the feasibility by modifying the existing breathing circuit to accommodate higher volumetric gas flows (±400 L/min) for exercise stress testing applications.

Several variations of the prototype systems were constructed. To increase the flow, a differential pressure flow transducer was obtained from a commercially available system used for exercise testing. The gas analysis sensors were then inserted into the main lumen at a $45^o$ angle so that the signal strength across the differential pressure drop was greater than 5 cm $H_2O$ at 400 L/min and produced minimal back pressure resistance.

Characterization of the flow required the use of a flow coefficient, indexed by the Reynolds number, to adjust for head losses created by the differential pressure sensor. With the flow coefficient adjustments, the accuracy of the flow compared to the theoretical flow value was within ±3% or ±1 L. A propane combustion chamber that simulated oxygen consumption was used to validate the luminescence-quenching oxygen sensor. The fraction of expired oxygen was determined theoretically based on the complete combustion of propane and compared to the actual recorded valued. The sensor was found to be accurate to within 6% across the range of flow.

TABLE OF CONTENT

# ACKNOWLEDGEMENTS

I would like to thank all those who have supported me in this endeavor. First, my committee members Dr. Dwayne Westenskow, Dr. Joseph Orr, and Dr. Rob MacLeod. Thank you for providing me with the opportunity to continue my education by providing the funding for the project and allowing me to work under your direction. Second, to all of my coworkers in the lab. Thank you for answering my endless questions and sharing your knowledge, especially of Matlab, with me. And third, to my wonderful friend and family. Thank you for encouraging me to pursue this degree and providing me with strength and support during the process. I love you all!

# CHAPTER 1

# INTRODUCTION

## 1.1. Objectives

Innovative technologies in the field of metabolic gas analysis sensors have resulted in smaller, lighter systems with rapid breath-by-breath analysis capabilities. These systems are currently utilized in patient care settings for the monitoring of relatively low flows of respiratory gases. The ratio of oxygen consumption and carbon dioxide production is used to estimate the body's total energy expenditure in a process known as indirect calorimetry. The motivation for this project was to determine the feasibility of modifying one such system, developed by Philips-Respironics, to accommodate the higher volumes of gas flow typically observed during exercise for the measurement of maximal oxygen uptake ($VO_2$ max).

The feasibility of engineering such a device is presented in this study as the following threefold specific aims: 1) build several prototype flow sensors that incorporate larger diameter tubing to reduce resistance to airflow during exercise while maintaining a differential pressure signal of 5 cm $H_2O$ at 400 liters per minute of flow, 2) calibrate the flow sensor and characterize flow measurements to within 3% of the measured oxygen concentration across a range of ±400 liters per min, and 3) determine the accuracy of the oxygen sensor on the bench using a propane combustion chamber.

## 1.2. Applications of Respiratory Gas Analysis

Monitoring the utilization of oxygen has long been of interest to scientists and clinicians because of its role in many important physiological processes. Simply put, inhaled oxygen is required for the metabolic reactions that produce molecules called adenosine triphosphates (ATP) where the cells store energy. Carbon dioxide gas is released as a byproduct and removed from the body during exhalation. As a result, the rates of oxygen consumption ($VO_2$) and carbon dioxide production ($VCO_2$) in respiratory gases directly correlate to the cell's metabolism of nutrients. On a broader scale, because several physiological systems are involved with the exchange, transport, and utilization of respiratory gases, monitoring $VO_2$ and $VCO_2$ is of interest for many different applications. The application of respiratory gas analysis can be divided into two main categories: diagnostic and monitoring.

Diagnostic respiratory gas analysis is used to determine the nutritional requirements for critically ill patients. Through a process known as indirect calorimetry, the basal metabolic rate, and hence the daily caloric burn rate, of a patient is estimated using predictive equations based on the rates of $VO_2$ and $VCO_2$. One often reported parameter obtained from gas analysis is the respiratory quotient (RQ). Defined as the ratio of $VCO_2$ to $VO_2$, the RQ of specific substrates has been well defined. Fats have an RQ = 0.7; while, on the other side of the scale, carbohydrates have an RQ = 1.0. Nutritionists use this information as a guideline to determine if a patient is being under- or overfed.[1]

Another application for diagnostic gas analysis is to measure the alveolar ventilation, uptake and distribution of anesthetics during surgery. The integrity of the gas

supply delivery system can also be tested to ensure there are no leaks and patients are receiving proper ventilation.

Respiratory gas analysis is also used to monitor changes in physical fitness. In the 1920s, researcher A.V. Hill introduced the concept of an oxygen plateau that occurs right before exhaustion during maximal exercise. The concept of maximal oxygen uptake ($VO_2$ max), which is described more fully in Section 1.6, has since become the most popular parameter used for quantifying an individual's overall physical fitness. It is also used to measure the effectiveness of specific training protocols. For more specific examples of monitoring respiratory gas analysis applications, see Chapter 5.

## 1.3. Gas Analysis Techniques

Historically, the analysis of respiratory gas exchange involved a technique developed by C. G. Douglas in 1911 in which exhaled air was collected in a large, impermeable canvas bag where it was available for subsequent analysis and volume measurements.[2] Fractional concentrations of expired oxygen ($FeO_2$) and expired carbon dioxide ($FeCO_2$) were determined using chemical absorption methods. Although this method was extremely accurate and is still often used for validation studies, the analysis was slow and required a skilled technician. Moreover, diffusion of gas through the fabric was a concern and rapid changes in ventilation or oxygen consumption ($VO_2$) were not visible.[3] It was not until the 1960s and 1970s that computerized systems, which featured integrated gas breath-by-breath analysis sensors and flow-sensing devices with automated breath recording, became available. Today there are dozens of automated gas analysis systems available on the market for both clinical and sports exercise applications.

These automated gas analysis systems employ various techniques for determining gas concentrations including mass spectrometry and substance sensitive sensors and detectors. The purpose of this section is to provide an overview of the technologies and discuss the applications and limitations of the different methods. It should be noted that the words sensor and detector are used interchangeably throughout this report.

### 1.3.1. Mass Spectrometry

Mass spectrometry (MS) is an analytical technique for determining the composition of a sample based on the masses of individual molecules. Mass spectrometers consist of an ion source, a mass analyzer, and a detector. First, the sample is loaded into the instrument where it is vaporized to form a gas. Then the sample is bombarded with an electrical beam that causes ions to form. Because ions are extremely reactive and short-lived, their formation is conducted in a vacuum. An electrical field is then applied to the sample, which causes the cations, formed in the previous step, to accelerate towards an electrode. Another perpendicular magnetic field deflects the ions. Based on the deflection trajectory pattern, the mass analyzer determines the mass-to-charge ratio of the sample.

Finally, the sample is collected by the detector and the ion flux is converted to a proportional electrical current. The information is converted into a mass spectrum and can be used to determine the concentrations of each species present. MS is capable of detecting very minute quantities (one part per billion). [4-6]

1.3.2. Metabolic Gas Analyzers

Metabolic gas analysis systems, or metabolic carts, are used to indirectly estimate energy expenditure through the continuous monitoring of respiratory gases.[7] In exercise physiology the measurements of $VO_2$ and $VCO_2$ are used to assess aerobic capacity during maximal exercise. In a clinical setting metabolic carts are often used to obtain information about gas exchange for anesthesia and to determine calorie requirements for bedridden patients.

These systems must be inexpensive, lightweight, robust, easily calibrated, simple to operate, and reliable. Unlike the Douglas bag method, modern metabolic gas analyzers are able to provide breath-by-breath analysis. Common features of all the devices include a spirometers for the measurement of gas flow, a carbon dioxide detector, and an oxygen sensor.[8] A brief description of the components is provided in the following sections.

1.3.2.1. Spirometers. Spirometers are used to measure lung function, specifically the volume or flow related to respiration as a function of time ($m^3/s$). This can be determined directly using traditional volume spirometers, or indirectly using a flow detector which derives the volume mathematically.

Direct spirometery records the rotation of a diaphragm when a breath is forcibly exhaled. The movement is traced on a moving paper graph where the volume is measured. There are three types of standard spirometers: the water seal, dry rolling seal, and bellow spirometers. Since spirometers are often large in mass, their use is impractical when measuring rapid changes in volume. For this reason they are not typically used for maximal exercise stress tests.[9]

For the indirect measurement of flow devices known as pneumotachometers are often used. Pneumotachometers rely on the principle that a drop in pressure is directly proportional to gas flow.[10] A computer integrates the flow over time to produce a gas volume. It should be mentioned there are four main types of pneumotachometers used in automated metabolic systems: differential pressure, turbines, Pitot tubes, and hot-wire anemometers. However, a further description of the different types is beyond the scope of the report. They are relatively inexpensive and can be disposable. While some criticize this method because volume is not measured directly, pneumotachometers are more robust and respond rapidly to changes in air flow, making them more suitable for exercise studies.

1.3.2.2. Carbon dioxide detector. Non-Dispersive infrared (NDIR) detectors are the most widely used method for the real-time measurement of carbon dioxide. Carbon dioxide absorbs infrared radiation at a specific wavelength due to the fundamental asymmetric O=C=O stretch. The sensor consists of an infrared (IR) source and a detector. Absorbance of the infrared light at 4.26 microns is proportional to the concentration of carbon dioxide. Most systems also have a reference signal, which detects the amount of light at a different wavelength where there is no absorbance.[11]

1.3.2.3. Oxygen sensor. Currently three main technologies are used in metabolic carts for oxygen concentration analysis: 1) semidisposable electrochemical sensors, 2) paramagnetic sensors, and 3) zirconium oxide oxygen sensors. A brief description of the technology is provided below.

Semidisposable electrochemical sensors use a galvanic fuel cell or polarographic (Clark) electrode to produce a stable current that is proportional to the partial pressure of

oxygen. These fuel cells have the advantage of being small, which makes them desirable for portable systems. The use of galvanic sensors in metabolic carts has been limited because they do not respond rapidly to changes in concentration, are expensive, and have a short electrode lifetime especially when exposed to high concentrations of oxygen. Polarographic sensors have a longer storage life than galvanic sensors, but require a significant amount of maintenance and upkeep.[12, 13]

Zirconium oxide fuel cells consist of a calcium-stabilized zirconium oxide electrolyte with porous platinum electrodes. At high temperatures (770-850 $^{o}$C), the zirconium lattice becomes porous and conducts the movement of oxygen ions from a higher concentration to a lower concentration. Typically one electrode is exposed to air and the other is exposed to the sample gas. The output voltage follows the Nernst equation and is relative to the partial pressure of oxygen. The sensor is extremely stable, precise over a wide range from 100% oxygen down to parts per billion, and capable of a fast response time. One major limitation is sensor fatigue, which results from the heating and cooling of the sensor. Also, at high temperatures, reducing gases (hydrocarbons of another species, hydrogen, and carbon monoxide) react with oxygen to produce a lower than actual oxygen reading.[14]

In a paramagnetic sensor, the magnetic susceptibility of oxygen is used to determine the partial pressure. In the 1800s Michael Faraday noted that the oxygen in a gas sample caused the rotation of a nitrogen-filled glass dumb-bell suspended in a magnetic field. The current needed to counteract the rotation is proportional to the concentration of oxygen. Today the systems consist of a light source, photodiode, and an amplifier circuit, which is used to measure the degree of rotation of the dumbbell. The

dumbbell is filled with an inert gas and suspended within a nonuniform magnetic field. When oxygen is present, the molecules are attached to the electromagnetic field and the dumbbell rotates. In addition to fast response times and the absence of consumable parts, the sensor has a good shelf life, making it the most utilized oxygen sensor. However, this method is not sensitive to trace amounts of oxygen.[15,16]

### 1.4. Limitations of Current Systems

In the 1980s and early 1990s mass spectrometers went from complex instruments that filled entire rooms to user-friendly bench-top devices. Further miniaturizing mass spectrometers has conventionally been limited by the vacuum and pump requirements. The ionization requirement destroys the sample, which is not desirable for all applications. Although there is rising interest in portable mass spectrometers for field studies, major manufacturers are concerned about limited markets and profit margins. Thus, mass spectrometers have remained relatively expensive when compared to metabolic gas analyzers.[17]

Computerized metabolic gas analyzers are often preferred over the Douglas bag technique because they can provide breath-by-breath information about gas exchange. However, several studies have shown there is wide variability in the reported parameters by the metabolic gas analyzers and there is still some debate about their accuracy. In a review of the automated systems, Macfarlane (2001) points out that these systems still have several shortcomings.[8]

First, the automated systems no longer require the user to have an understanding of how the data is generated. This creates conceptual and technical problems during data

analysis. Second, oxygen and carbon dioxide sensors are sensitive to the presence of water vapor. Water vapor can condense in the sampling line where it must be removed before it reaches the sensor. Another challenge is keeping the partial pressure of water vapor the same during the calibration and measurement phases to obtain the correct results for dry gas concentrations.

The third problem, which Macfarlane suspects is the greatest of the three, is that the automated systems require an exact alignment of the flow and gas analysis signals. Many systems utilize a mixing chamber for steady-state gas analysis. This method creates a lag between the gas analysis signal and the flow signal, which must be realigned for breath-by-breath analysis.

### 1.5. Innovation of Luminescence Quenching Oxygen Sensor

Recently Phillips-Respironics (Phillips, Carlsbad, California) introduced an innovative technique, based on the principle of luminescence quenching, for the measurement of oxygen to be used in their clinical metabolic cart known as the NICO Respiratory Profile Monitor.

The instrument consists of a light emitting diode that serves as the excitation source for a luminescent dye. A photosensitive detector is mounted in a position to respond to the filtered fluorescent radiation emerging from the exit optical filter. The oxygen sensor, contained in a cuvette along with a NDIR $CO_2$ analyzer, is comprised of a thin film of transparent material containing the luminescent dye where rapid diffusion of molecular oxygen from the airway gas environment takes place. The system is more rapidly depleted of the excited-state dye molecules when oxygen is present, making the

oxygen concentration proportional to the amount of quenching observed. Simply, when oxygen is not present in the system, more fluorescence is observed than when oxygen is present in the system.

A short pulse of light illuminates the film 100 times a second and the system analyzes the magnitude and phase of the resulting excitation following each pulse. Each pulse provides a sample of the oxygen signal. This oxygen signal is presently designed to give a simple oxygen waveform and measurement of inspired and expired oxygen with the existing flow signal to calculate oxygen uptake.

The accuracy of the luminescence quenching technique for oxygen analysis in a critical care environment was performed in the lab using a patient lung simulator. Through the combustion of propane, which occurs in a sealed chamber, the exact amount of $VO_2$ and $VCO_2$ and water vapor production can be determined. When compared with the oxygen consumption measured by the sensor, the accuracy was found to be within -0.3±2.8%.[18]

Further validation of the sensor was performed in a clinical trial using 20 (10 female, 10 male) human volunteers at rest. When compared against the clinical gold standard device (DeltaTrac, Datex, Helsinki, Finland) an error in oxygen consumption measurement of 2.2±4.1% and an error 1.63±4.41% in carbon dioxide production measurement was found.[19] The system was also tested on 14 intensive care unit (ICU) patients and found to be within 1.7±6.9% of the reference analyzer.[20]

In a clinical setting with respiratory gas flows of less than ±180 L/min, this novel sensor offers many advantages over previous methods for determining oxygen concentration. The sensor can be placed directly on the airway instead of a side stream

so that real-time oxygen consumption is possible. This eliminates the need for aligning the flow and breath signals and water condensation in the hoses of the drawn sample. Due to its light sensitive properties, the sensor is subjected to photo bleaching over time. However, the sensors are relatively cheap and are not difficult to replace.

### 1.6. Motivation for Development of a Portable Metabolic System

Up to this point the utilization of luminescence quenching technology has been primarily focused on its benefits in metabolic analysis systems in a clinical setting, but there is a growing demand for a portable gas analysis system to be used as part of a routine health monitoring. Once only a small portion of athletes used exercise stress testing to determine their fitness levels. Now every day exercise enthusiasts are interested in parameters obtained from gas analysis, primarily maximal oxygen uptake. Similarly, popular televisions shows that feature gas analyses as a way to determine and track daily energy expenditure have increased the demand for gas analysis as a weight loss tool. While there are a few portable gas analysis systems available, most rely on galvanic fuel cells for oxygen analysis. The purpose of this research is to extend the use of luminescence quenching technology by developing a prototype metabolic system that could be used during exercise testing.

The following section provides an overview of exercise stress testing including the definition of maximal oxygen uptake, how it is determined, and the expected ranges for different athletes. As discussed earlier, the determination of energy expenditure is straightforward based on the ratio of oxygen consumption to carbon dioxide production.

## 1.7. Exercise Stress Testing

### 1.7.1. Maximal Oxygen Uptake (VO2 Max)

The most commonly measured parameter during exercise stress tests is maximum oxygen uptake ($VO_2$ max). During exercise, the several physiological systems must work together in order to provide the body with the nutrients, including oxygen for the production of ATP, needed to sustain the activity. At some point during maximal exercise the linear relationship between $O_2$ consumption and mechanical power plateaus. This point, known as $VO_2$ max, is considered the best indicator of cardiorespiratory endurance and aerobic fitness. Consequently, measuring $VO_2$ max is of interest to athletes and others seeking to monitor their cardiovascular fitness.

Maximal oxygen uptake is largely influenced by three major factors: cardiac output, the oxygen carrying capacity of the blood, and the amount of exercising skeletal muscles and the ability of those muscles to utilize the supplied oxygen.[21] Other factors include age, gender, altitude, and overall physical health. Some estimates say that genetics and heredity account for nearly 25-50% of the variance in $VO_2$ seen between individuals.[22,23] Some of these factors do not change with exercise, but endurance training can greatly increase the ability of aerobic enzymes to extract oxygen from the blood.[24] The type of muscle fiber is also important. Briefly, slow twitch muscle fibers are naturally more oxidative, and have more mitochondria and capillaries than the fast twitch muscle fibers developed during strength training. This allows the muscles to better utilize the oxygen from the blood.[25]

1.7.2. Measurement

To determine the $VO_2$ max, respiratory gas flow and the concentration of inspired and expired oxygen and carbon dioxide must be recorded simultaneously while the subject is performing a specific exercise protocol. The breathing circuit is attached to a headpiece, which must be worn during the exercise test. Room air, which contains 20.93% oxygen and 0.03% carbon dioxide, is inhaled through a non-rebreathing valve. When the subject exhales, the gas travels through the breathing circuit to a metabolic cart where gas analysis occurs. After the concentration of oxygen in the inspired air is adjusted for barometric pressure, humidity, and temperature, oxygen consumption can be determined.

The classic protocol for $VO_2$ max testing involves exercising on a treadmill or stationary ergometer. The intensity of the work load increases at periodic intervals until the subject is exhausted and cannot continue. This usually occurs after about 10-15 minutes of exercise. A true $VO_2$ max reading requires a trained test administrator and a highly motivated individual. Sometimes there is not a clear plateau observed. In these cases, secondary criteria including high levels of lactic acid in the blood, an elevated respiratory exchange ratio, and some percentage of an age-adjusted maximal heart rate are used to determine the exact point of $VO_2$ max. $VO_2$ max can also be estimated using predictive equations based on heart rate and work rate.

1.7.3. Average Range for Normal Individuals

Because oxygen and energy requirements vary with body type and size, $VO_2$ max is often expressed in ml $O_2$/kg/min. A typical human at rest requires 3.5 ml $O_2$/kg/min

for just for cellular activities. The average $VO_2$ max for an untrained 40 year old male is in the range of 35-40 ml $O_2$/kg/min. In general, a female of the same age would have a value around 30-35 ml $O_2$/kg/min. By contrast, cyclist Lance Armstrong has a reported $VO_2$ max of 83-85 ml/kg/min; Steve Prefontain, an elite runner; 84.4 ml/kg/min; Bjorn Daehlie, a Norwegian cross country skier, 90.0 kg/ml/min; and female marathon runner Joan Benoit, 78.6 ml/kg/min. A Scandinavian cross country skier is reported to hold the record for the highest $VO_2$ max at 94 ml/kg/min.[26]

## 1.8. Overview of Thesis

The ultimate goal of this project was to determine the feasibility of developing a prototype gas analysis system that incorporated a luminescence quenching $O_2$ sensor, a NDIR $CO_2$ sensor, and a fixed orifice differential pressure flow meter. Each of these components has been successfully used individually or in combination for clinical applications, but together the three pieces have not been used for monitoring gas analysis applications such as exercise stress testing. To evaluate the prototype system, the project was divided into three stages.

In the first stage, presented in Chapter 2, three criteria were established for the design of the prototype system. Several prototype metabolic gas analysis systems with different sensor configurations were constructed. The designs were tested to ensure that enough gas flow reached the sensor for adequate analysis. Back pressure resistance and flow signal were also measured. A discussion of each design and its performance is included. The commercial requirements for back pressure resistance and flow signal are also discussed, and the best design was selected.

In the second phase, Chapter 3, the flow sensor was calibrated using a correction factor known as the discharge coefficient. The use of indirect flow measurement by means of a fixed orifice differential pressure transducer is discussed. The derivation of the flow equations using the Bernoulli equation and the discharge coefficient theory are also presented. The coefficient was determined and the accuracy of the prototype flow sensor using the discharge coefficient is given.

In the last stage, Chapter 4, the accuracy of luminescence quenching oxygen sensor was tested on the bench using a propane combustion patient simulator. The combustion of propane requires a fixed amount of oxygen. This amount was then compared to the measured amount of the oxygen in the gas from the chamber by the sensor. A discussion of the experimental design limitations concludes the research section.

Finally, in the closing chapter the results are again summarized. Limitations of the methods used in the study are presented including any future work that is necessary before the prototype system could be developed commercially. A few possible applications are suggested. A summary of the overall findings concludes the project.

# CHAPTER 2

# PROTOTYPE DESIGN

## 2.1. Introduction

Luminescence quenching has been used successfully in a critical care environment. With a few modifications it was proposed that the applications could extend to monitoring applications. As part of a collaborative effort between Phillips-Respironics and Dr. Joseph Orr and his research group at the University of Utah, a compact flow measurement system complete with the hardware and algorithms needed for measurement of $VO_2$ and $VCO_2$ was developed. The technology is currently marketed by Phillips under the trade name FloTrac Elite. Because of its compact size it is ideal for a portable metabolic gas analysis system. However, its use in exercise testing is currently limited by the diameter of the tubing and the volumetric flow it is capable of handling. The purpose of this stage of the project was to modify the flow sensor housing so that more airflow was available.

This chapter includes a description of the terminology used when designing the breathing circuit, the desired criteria and methods for testing each exercise prototype breathing circuit, the results including end-tidal $CO_2$ ($ETCO_2$), back pressure, and resistance tests, and a discussion of the selected prototype and its performance. The units of volumetric flow are given in liters per minute (L/min) and liters per second (L/s).

## 2.2. Description of Terminology

There are three main components of the prototype gas analysis system: 1) the breathing circuit, which is made up of the on-airway luminescence quenching $O_2$ sensor, NDIR $CO_2$ analyzer, and the differential pressure port housing, 2) the FloTrac Elite, which is the module containing the algorithms required for the gas analysis, and 3) the Capnostat, which is connected to the FloTrac Elite and acts as the excitation source and detector for NDIR $CO_2$ and $O_2$ analysis.

A schematic of a portion of the breathing circuit is shown in **Figure 2.1**. The sensor consists of a gas cuvette with a coupling on either side. The capnostat attaches to the cuvette. As the sampled gas travels through the cuvette the capnostat detects the $O_2$ and $CO_2$ molecules present and relays the information to the FloTrac Elite for signal processing. The gas cuvette was inserted into the main lumen of the flow housing device well after the pressure ports. The exhaled flow was then directed either out of the main flow orifice or across the sensor.

Based on the orientation of the sensor in this study, gas flow first enters the smaller diameter coupling (~13 mm), moves through the sampling chamber in the cuvette, and exits the larger diameter coupling (~16 mm). Hence, each coupling will be distinguished as the input and output coupling, respectively.

The housing for the differential pressure flow sensor was obtained from a CardioCoach Fitness Assessment Analyzer (Korr Medical, Salt Lake City, Utah). The oxygen and carbon dioxide sensors were provided by Phillips-Respironics (Phillips-Respironics, Carlsbad, California). The pressure differential drop was created by a slight constriction in the main lumen of the flow located in between the two ports. The

standard pressure ports included on the housing were connected via tubing to the pressure transducer also located in the FloTrac Elite. The FloTrac Elite outputs the drop as a volumetric flow using computer algorithms.

The gas flow path is shown in **Figure 2.1** in red. Only the portion of the sensor utilized when the subject exhales is shown. The headpiece worn by the subject and the mask including the inhalation non-rebreathing valve is not pictured.

## 2.3. Prototype Design Criteria

Three criteria were considered when designing a prototype on-airway gas analysis system. First, the expected respiratory flow for a patient in the intensive care unit (ICU) is small – no more than 180 L/min at a maximum. Thus, only a small diameter (<15 mm) is required for the lumen of the breathing circuit to meet the airflow requirements. During exercise a healthy adult requires air flows in the range of 400 L/min. The prototype breathing circuit for an exercise metabolic gas system must feature a larger diameter lumen that is capable of handling these flows.

Modifying the sensor cuvette could have potentially damaged the integrity of the sensor, so it was decided the best approach would be to create a branch to divert some of the flow across the sensor and allow the remaining flow to exit with minimal resistance. To ensure that enough gas was reaching the sensor for adequate gas analysis, the end-tidal $CO_2$ ($ETCO_2$) at the test site was recorded and compared to a reference location. The geometry which provided a minimal difference in $ETCO_2$ would be selected.

Second, because the system uses a differential pressure type flow sensor, a compromise between the back pressure flow experienced by the user and the magnitude

of the transducer signal produced from the pressure drop was required.[8] For a strong signal-to-noise ratio a large differential pressure in response to gas flow was desirable. In industry, a differential pressure signal of at least 5 cm $H_2O$ at 6.6 L/s is considered acceptable.

Finally, the most effective prototype would provide adequate airflow to the sensor for gas analysis without introducing unnecessary back pressure and hence resistance, which may lead to premature $VO_2$ max readings. The American Thoracic Society (ATS) issued a policy statement recommending that the upper limit for resistance and back pressure for a monitoring spirometers at <2.5 cm $H_20$/L/s ±14L/s over the flow range.[27, 28]

## 2.4. Materials and Methods

### 2.4.1. Prototype Breathing Circuits

Several prototype breathing circuits were designed using three fundamental sensors with additional modifications made to each. A description of the three sensors and the modifications made to each are given in **Table 2.1**. To prevent back diffusion across the sensor from the output coupling, resistance in the form of addition length was added. No further modifications were made to the outlet coupling. Thus the description of the modification in **Table 2.1** refers solely to changes made to the input coupling. The sensor was then inserted at a $90^o$ angle into the lumen of the flow sensing device.

In the first series of prototype circuits using the first base sensor, no further modifications (**1A**) were made to the actual standard sensor housing as shown in **Figure 2.2**. The input coupling had the following dimensions: from the base of the sensor cuvette the coupling extended 17.9 mm, had an outer diameter of 15.3 mm, an inner

diameter of 13.3 mm, and a thickness of 1 mm. The input coupling tapered slightly so that the circumference at the most distal portion from the base of the cuvette is 48 mm.

The additional modifications added to this series of prototypes consisted of restrictions made to the main flow exit orifice. A schematic of the top view of the main flow orifice opening is given in **Figure 2.3.** The flow paths are indicated by the red arrows. The flow orifice proximal to the sensor was covered in the modifications **1B-1E** so that the flow was allowed to exit through the most distal opening and through the output coupling on the sensor. In **1F-1G**, the flow orifice proximal to the sensor was uncovered and the covering was placed on the distal side.

In the second series of prototypes, the basic sensor had a 10.7 x 16.9 mm rectangular portion of the coupling wall removed 8.4 mm from the base of the cuvette so that the remaining circumference was 31.2 mm. The sensor was positioned in such a way as to help direct more flow to the sensor. As in the previous series, similar modifications to the flow orifice were made in **2B-2D**. The last two modifications were an addition of length and the remaining circumference **2E-2F**. A rendition of the Sensor #2 and the last two modifications is given in **Figure 2.4**.

For the base sensor in the third series of prototypes, the extension of the input coupling on a standard sensor was shortened. Then various modifications were made to the extension and circumference as outlined in **Table 2.1**. **Figure 2.5** shows a rendition of the sensors arranged by the length of the extension (from the most to the least).

Based on the results of the all three series of prototypes, a final base sensor with a 25.4 mm extension to the inlet coupling was inserted into the flow at a $45^{o}$ angle. A rendition of this prototype is included in the results portion.

2.4.2. Flow Diversion – End-Tidal $CO_2$

To determine the efficacy of the each design, each prototype was connected to a test lung, **Figure 2.6**. At the base of the test lung was a reference sensor. The lung was powered with an ESPRIT ventilator (Phillips-Respironics, Carlsbad, California), with the settings shown in **Table 2.2**. Carbon dioxide levels were set so that the end-tidal carbon dioxide ($ETCO_2$) was between 34-36 mm Hg, within an acceptable range for human $ETCO_2$. The mechanical lung provided a tidal volume for each breath of 1 liter.

Flow Host software was used to record the flow parameters. After a one-minute stabilization period the $ETCO_2$ was recorded for five breaths on the reference sensor. The process was repeated for the test site and again at the reference site.

2.4.3. Signal Strength and Back Pressure Resistance

A sensor design that met the aforementioned $ETCO_2$ criteria was selected. The sensor was then tested to ensure that a user would experience minimal back pressure resistance when breathing through the circuit and that the differential pressure drop produced a strong signal. For a baseline reference, the standard housing for the differential pressure flow sensor obtained from Korr Medical was also tested. The experimental setup is shown in **Figure 2.7.** Constant air flow at ambient conditions was provided by an ESPRIT Ventilator (Phillips-Respironics, Carlsbad, California). The ventilator was connected to the high flow input on a VT Plus Gas Flow Analyzer (Bio-Tek, Winooski, Vermont), which was used to verify the flow rate. The VT Plus was calibrated using a 3 liter syringe. The flow sensor was connected to the high flow exhaust on the VT Plus. The sensor was connected to the FloTrac Elite and then to a

laptop. NICO Data collection software recorded differential pressure signal. The average flow ranged from 2-300 L/min.

## 2.5. Results

### 2.5.1. Flow Diversion – End-Tidal $CO_2$

The $ETCO_2$, given in mm Hg, for the reference, test, and reference sites for each base sensor and its modifications are presented. For a description of each base sensor and its modifications refer to **Table 2.1**. The percent error, defined as the difference between the test site and the average of both reference sites over the average of both reference sites for the measured $ETCO_2$ (mm Hg), is given in the last column.

For the first series, the $ETCO_2$ measurements are given in **Table 2.3** and **Figure 2.8**. When no modifications were made to the sensor an $ETCO_2$ measurement could not be obtained. When a covering was placed over the main flow orifice so that all the air was forced the sensor, the $ETCO_2$ at the reference site measured higher than at the test site. When the flow orifice was only partially covered proximal to the sensor so that some air flow was allowed to pass through the distal side of the flow orifice, a similar pattern was observed. When the cover was moved to the distal side so that the air flow could pass proximal to the sensor the test $ETCO_2$ measured higher than at the reference site.

In the second series a portion of the inlet coupling was removed. This was thought to help lower back pressure resistance and promote gas flow to the sensor, **Table 2.4** and **Figure 2.9**. With no modifications, the base Sensor #2 had a significantly lower reading at the test site than the reference site. When portions of the flow orifice were

covered the results were similar to the first series. Once the covering was removed and the inlet coupling was extended further into the flow housing lumen, the reference readings increased and the test site readings decrease.

A third series of sensors using the base sensor #3 with a shorted input connector were tested. The $ETCO_2$ reading between the test and reference site seemed to be a function of the extension added to the input connector, **Table 2.5** and **Figure 2.10**. As length was added the difference between the reference and test site $ETCO_2$ measurements decreased.

A rendition of the final sensor with the capnostat attached is shown in **Figure 2.11**. To optimize the possible length extension a sensor was inserted at a $45^o$ angle into the main flow. A portion of the input connector wall was removed to facilitate air flow across the senor and an extension to the inlet coupling of 7.52 mm (25.4 mm from the base) was added. When the $ETCO_2$ of this sensor was tested there was a minimal difference between the reference site and the test site, **Figure 2.12.** The average partial pressure of $ETCO_2$ for 5 breaths (mean ± standard deviation) at the reference site, test site, and reference site was 35.8±0.08, 35.7±0.08, and 35.8±0.08 mmHg, respectively. These findings were repeated 3 times and the $ETCO_2$. The standard error between the test and reference location was 0.12%.

### 2.5.2. Differential Pressure Signal Strength

All analysis was conducted using Microsoft Excel 2003. The VT Plus was calibrated using a 3 liter syringe and found to have a percent error of ± 0.83%. All experiments were conducted at ambient conditions (room temperature = 75.9, relative

humidity = 20%, barometric pressure = 635 mm Hg). By the National Institute of Standards Technology's (NIST) definition of standards conditions, a temperature of 20$^{o}$C and pressure of 760 mm Hg were used in the calculations.

The differential pressure signal (cm$H_2O$) was recorded at flow rates of 0 to 300 L/min, **Figure 2.13**. The standard differential pressure housing was tested on flow rates from 0 to 165 L/min, and is referred to in **Figure 2.13** as the baseline. At low flows differences in the baseline and modified breathing circuit differential pressure signal strength are minimal. As the volumetric flow rate was increased the differential signal strength improved in the modified breathing circuit.

The back pressure resistance (cm $H_20$/L/s) that a user would experience is given in **Figure 2.14**. Again, at low flows deviations in the baseline and modified breathing circuit resistance are minimal. However, as the flow increased the back pressure resistance in the modified circuit became more noticeable. Based on the trend line equation shown on the graph, the resistance to back pressure was extrapolated out to 6.67 L/s (400 L/min) and found to be 2.87 cm $H_20$/L/s for the baseline and 3.14 cm $H_20$/L/s for the modified breathing circuit.

## 2.6. Discussion

The intent of these experiments was to develop a breathing circuit that could be worn during cardiovascular fitness testing that would feature minimal back pressure resistance while also providing a large differential pressure signal. Since variations in sensor geometry have been shown to greatly affect the velocity profiles and can lead to

significant errors in flow measurements, several different sensors geometries were tested to determine which design best fulfilled the specified criteria.[11]

In the first experiment $ETCO_2$ was monitored to ensure that enough sample gas flow was diverted to the sensor from the main flow to produce an accurate flow reading. One $CO_2$ sensor at the base of the breathing circuit was used as a reference. Another sensor branched from the main flow was used to measured the $ETCO_2$ as it would be placed in the breathing circuit. The sensor with a minimal difference in $ETCO_2$ readings between the reference and test sites was selected.

When a standard sensor with no modifications was placed at a $90^o$ angle into the main flow no $ETCO_2$ readings at the test site could be obtained. The small diameter of the input connector produced too much resistance and the flow continued through the unrestricted main flow orifice. When the main exit orifice outlet size was partially obstructed more flow was forced across the sensor.

The difference in $ETCO_2$ and percent error between the reference and test site was influenced by the orientation of the covering. When the flow was allowed to pass through the orifice opening distally from the sensor, the $ETCO_2$ measured lower at the test site than at the reference site. When the orifice opening proximal to the sensor was left open, the $ETCO_2$ read higher at the test site than at the reference site. Most likely the later configuration caused a change in the partial pressure within the sensor, thus altering the $ETCO_2$ at the test site. Further evidence of this theory is seen by the drop in the $ETCO_2$ at the reference locations when the flow orifice was completely blocked. Regardless of the orientation, there was still a significant difference between the test and

reference site. Moreover, by covering the main flow orifice extra resistance was introduced into the breathing circuit and those designs were discarded.

Another series of designs featured a modified inlet connector. A portion of the inlet connector was removed to decrease resistance. By removing different portions of the inlet circumference and adding additional length to the end sensor it was found the difference in reference and test $ETCO_2$ became less significant. To further decrease resistance, the sensor was inserted into the flow at a $45^o$ angle so that after the differential pressure ports the breathing circuit split into a wye piece with one larger diameter branch and one smaller diameter branch with the sensor attached. This design proved to be the most successful.

One disadvantage of the existing metabolic analyzers is the discomfort experienced by the user when trying to breathe through the circuit. Several studies have investigated how resistance affects the $VO_2$ max reading.[29-31] Deno et al. (1981) recorded $VO_2$ max for short and long duration exercise protocols. They found that a certain amount of resistance could be tolerated and did not reduce the $VO_2$ max. After a point, however, the $VO_2$ max reported dropped proportional to the resistance added.[32] Therefore it is important that the back pressure resistance caused by the system is minimized.

Another factor that must be balanced with the back pressure resistance is the signal strength. Early differential pressure transducers were noisy and had low analog-to-digital resolution at low flows. Newer generations have improved, but for maximum resolution it is still desirable to have signal strength of at least 5 cm $H_2O$ across the range of the flow.

The prototype flow sensor calibration showed a strong signal strength while remaining a flow resistance of <3.5 cm $H_2O$/L/s at 6.6 L/s, higher than the recommended ATS value. The standard housing casing for the differential pressure ports was also obtained from Korr Medical and tested as a baseline. As shown in **Figure 2.14**, the back pressure resistance measured in the modified breathing circuit was slightly higher than the baseline circuit. Future work will include optimizing the back pressure resistance to signal strength, but the results demonstrated satisfactorily that a breathing circuit using luminescence quenching for exercise purposes could be constructed

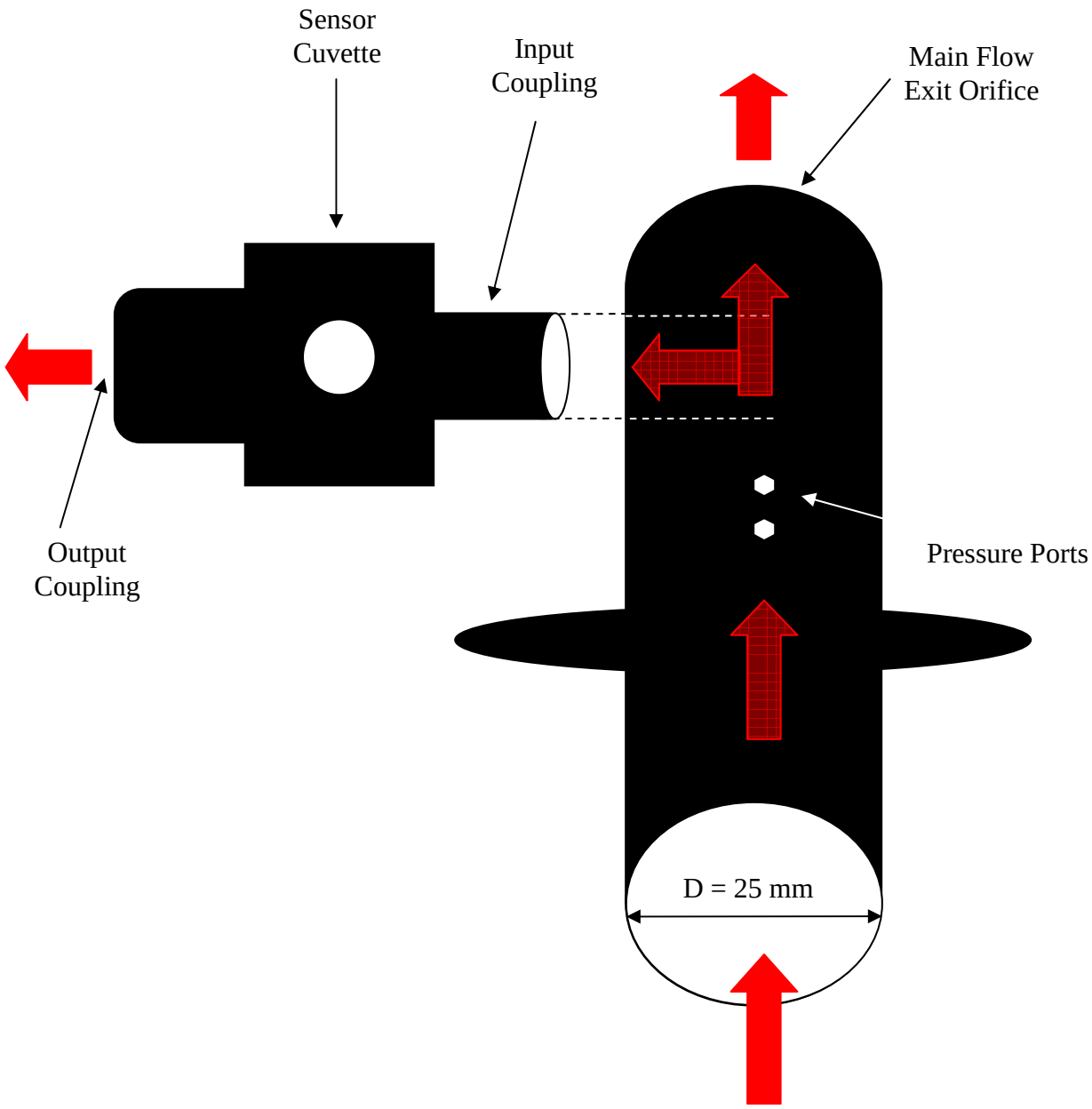


**Figure 2.1** 2D schematic of the components for the exhaled air breathing circuit. The sensor consisted of an output and input coupling and the main cuvette where the Capnostat attaches. The flow housing device features a large diameter to accommodate high air flow during exhalation, pressure ports for the recording of the differential signal drop caused by an obstruction to flow, and the main flow exit orifice. The sensor was inserted into the main lumen of the breathing circuit just beyond the pressure ports. The airflow path is marked by the red arrows. The capnostat, FloTrac Elite, and the restriction between the pressure ports which causes the pressure drop and are not pictured.

**Figure 2.2** The standard sensor with no modifications inserted into the flow sensor housing

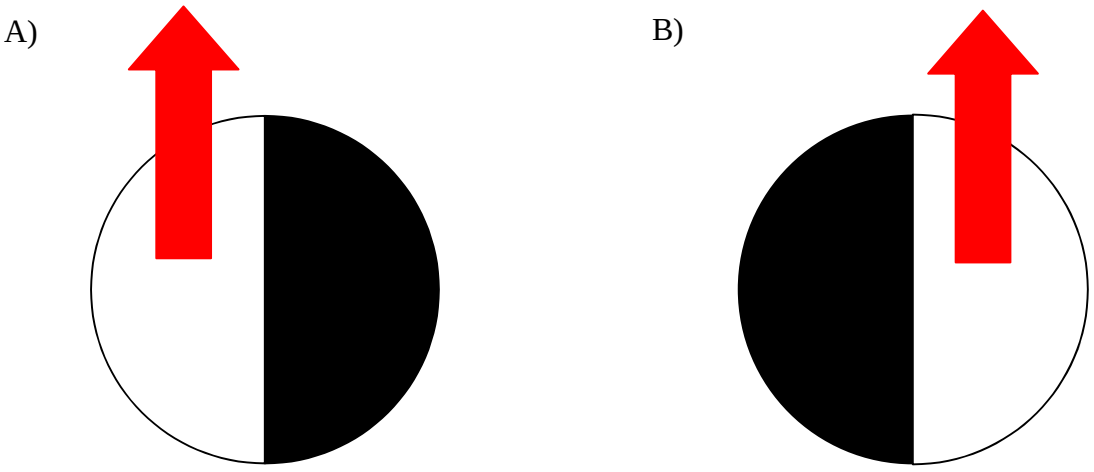


**Figure 2.3** Top view of the modifications made to the main flow orifice. The sensor was inserted on the left side. A) The portion of the orifice distal to the sensor was blocked. B) The portion of the orifice proximal to the sensor was blocked.

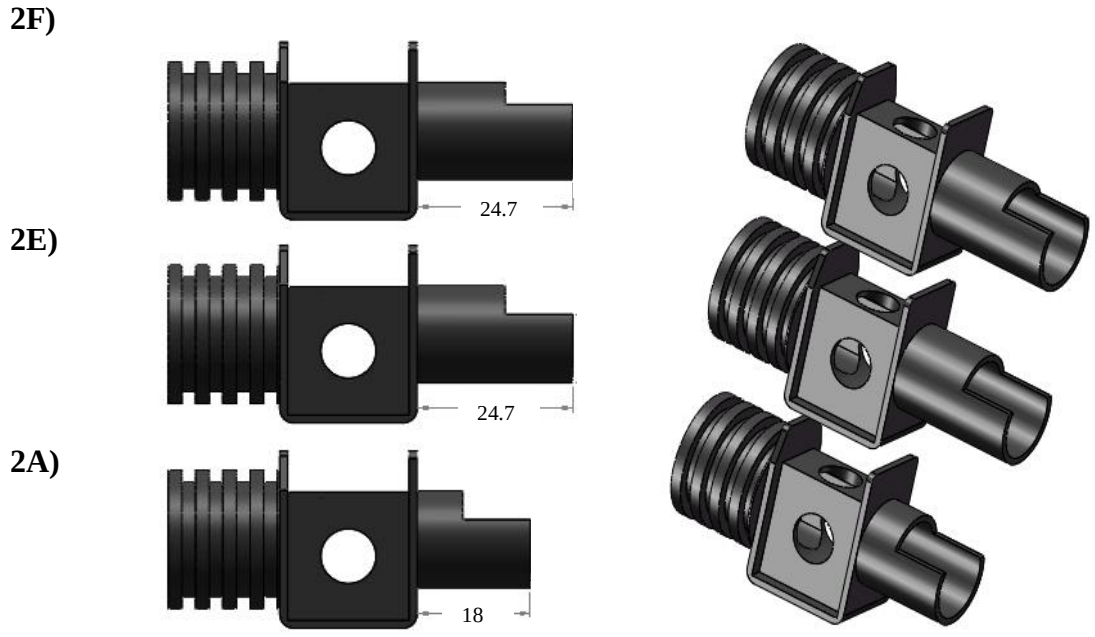


**Figure 2.4** Sensor #2 and the modifications made to the extension length and circumference (1E-1F) in mm.

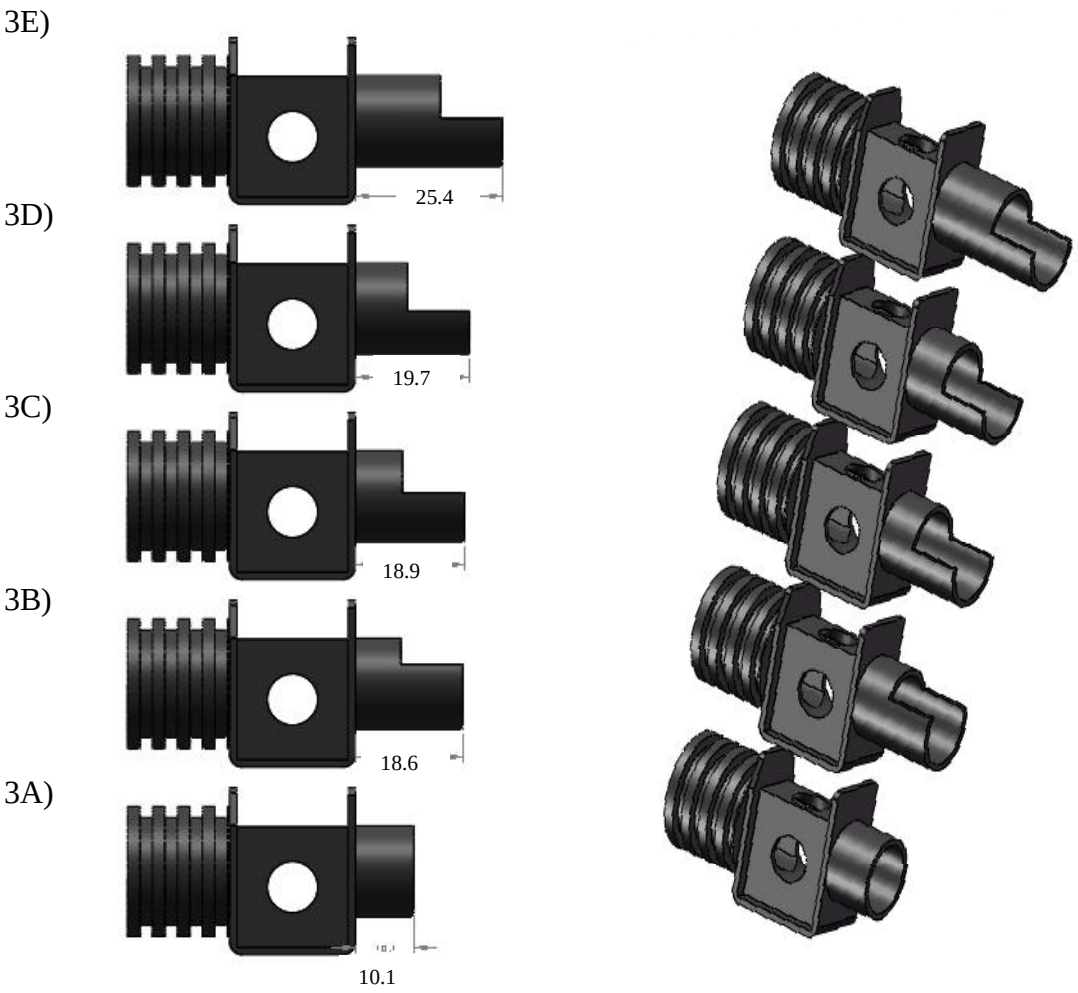


**Figure 2.5** Sensor #3 and the modifications in order of decreasing extension length in mm. For a further description of the modifications refer to **Table 2.1**.

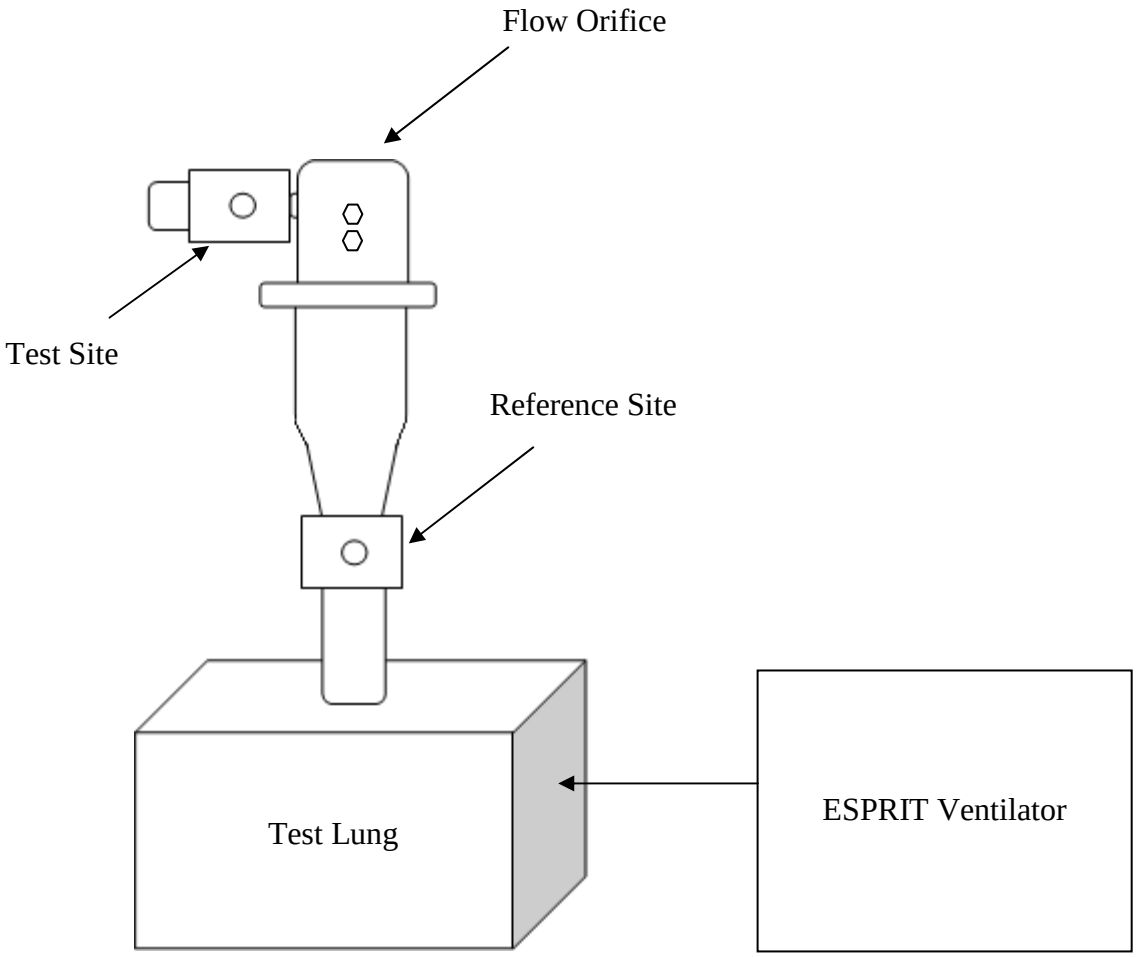


**Figure 2.6** Experimental setup for flow diversion to the sensor. $ETCO_2$ was recorded at the reference site and the test site. Ideally there should be a minimal difference in $ETCO_2$ between the two sites if enough air flow is reaching the sensor.

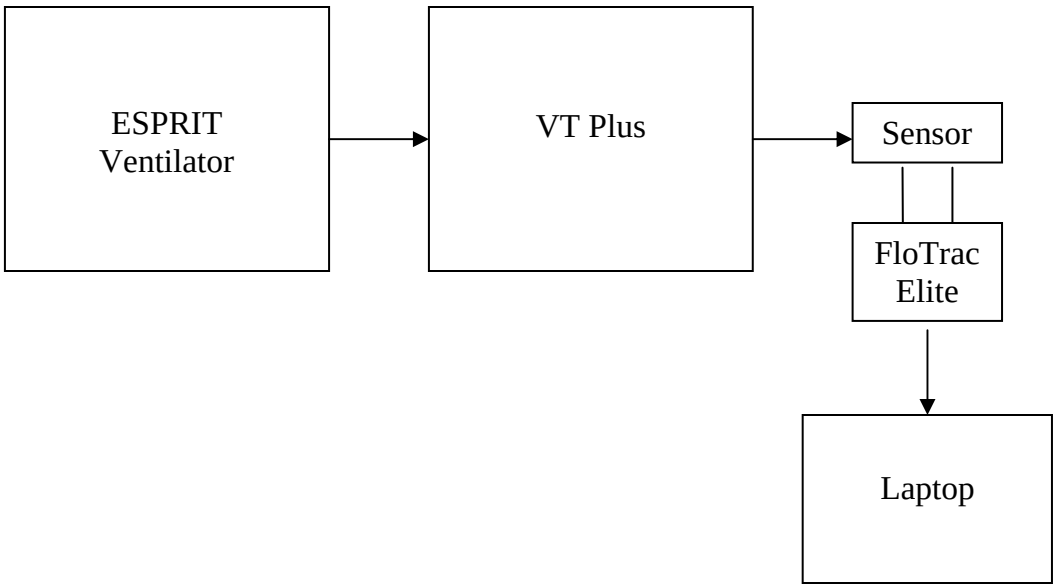


**Figure 2.7** Experimental setup for signal strength and flow resistance measurement

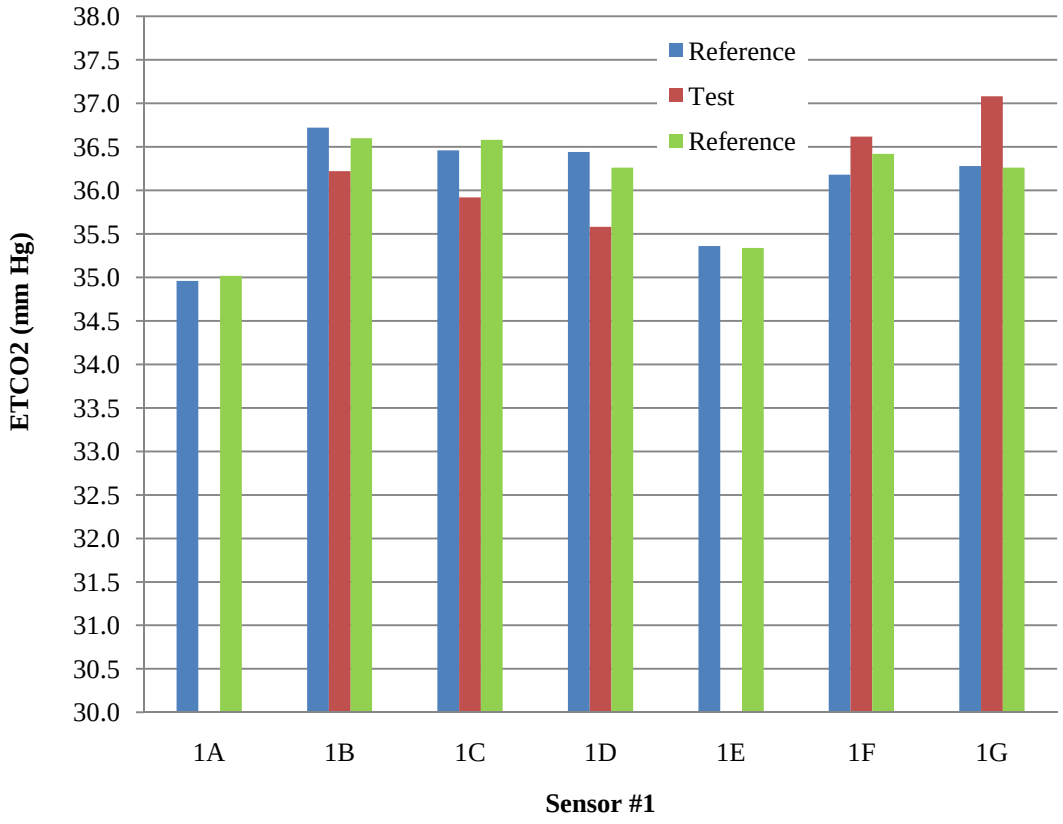


**Figure 2.8** $ETCO_2$ for the first series of sensors using base sensor #1. No modifications were made to a standard sensor (1A) and not enough flow reached the sensor. A covering was placed over the proximal portion of the main flow orifice (1B-1E) to force flow across the sensor. A covering was placed over the distal portion of the sensor (1F-1G). While covering the main flow orifice did help, this was not a desirable option as it added unwanted resistance to the breathing circuit.

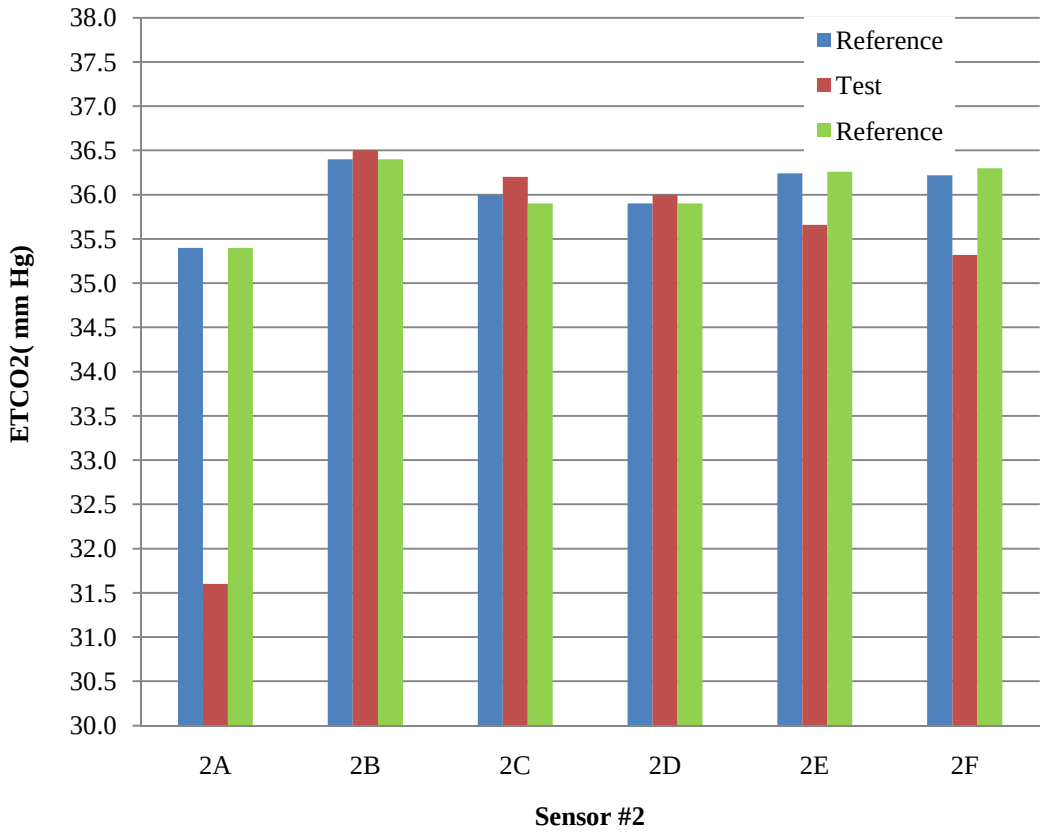


**Figure 2.9** $ETCO_2$ for second series using base sensor #2 and its modifications**.** Sensor #2 with no additional modifications (2A) had an $ETCO_2$ at the test site that was significantly lower than at the reference site. When the main flow orifice was partially blocked, the trend was similar to the first sensor (2B-2D). When the covering was removed and the length of the input connector was extended (2E-2F), the $ETCO_2$ at the reference site was higher than at the test site.

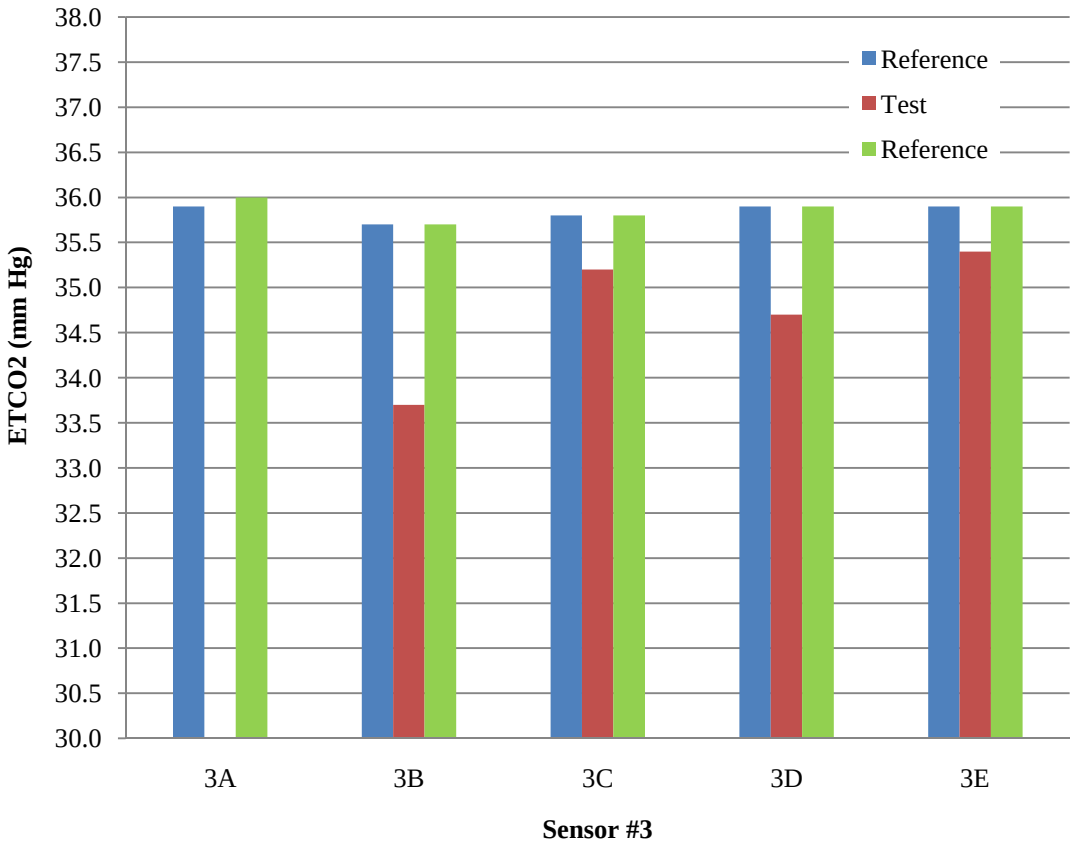


**Figure 2.10** $ETCO_2$ for the third series using base sensor #3 and its modifications. No modifications were made to the third base sensor (3A). When the covering was removed and the length of the input connector was extended, the $ETCO_2$ at the reference site was higher than at the test site in all cases (3B-3E).

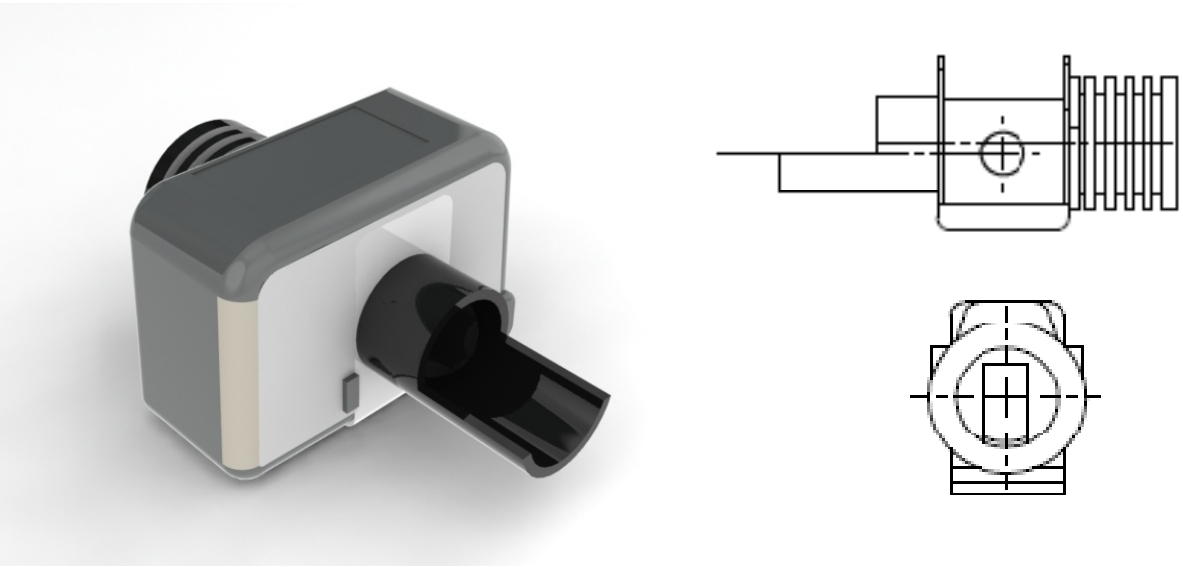

**Figure 2.11** A rendition of the final $CO_2$ sensor with the capnostat attached. The sensor was inserted into the main flow at a $45^o$ angle. A portion of the input connection was removed to reduce resistance. The remaining portion was extended to help guide the flow to the sensor.

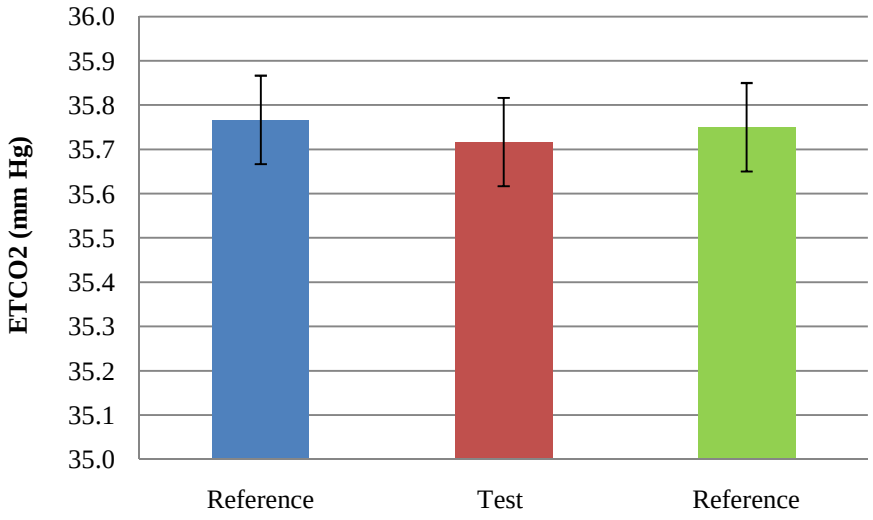


**Figure 2.12** The average partial pressure of $ETCO_2$ for 5 breaths (mean ± standard deviation) at the reference site, test site, and reference site was 35.8±0.08, 35.7±0.08, and 35.8±0.08mmHg, respectively. The error between the average of both references and the test location was 0.12%. These findings were repeated 3 times and the $ETCO_2$ was consistently found to be within an acceptable range.

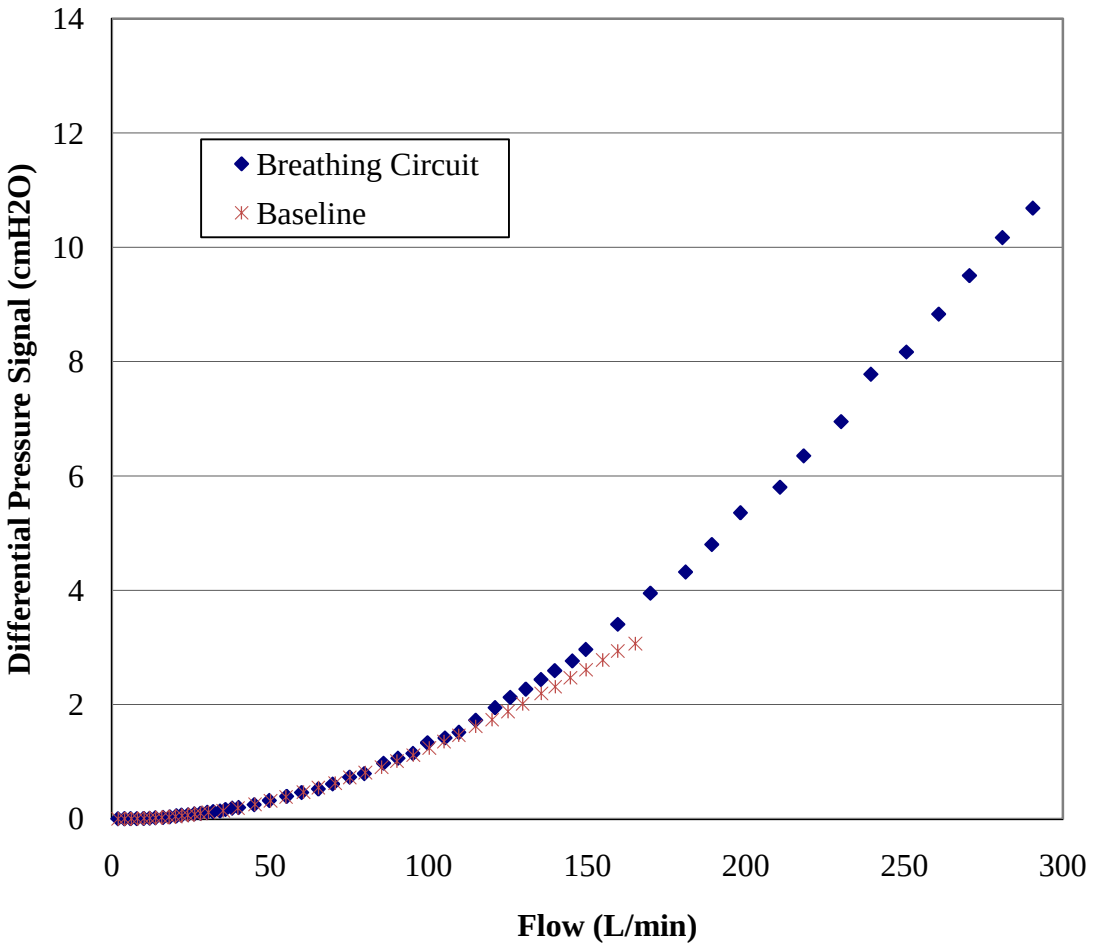


**Figure 2.13** Differential pressure signal (cm $H_20$) at flows ranging from 0-300 L/min. At low flows the differential pressure was much more sensitive to noise, so it was necessary to gather data at 2 L/min increments. At 300 L/min the flow signal generated from the tranducer was greater than 5 $cmH_2O$, large enough for the flow signal to be determined independent of noise.

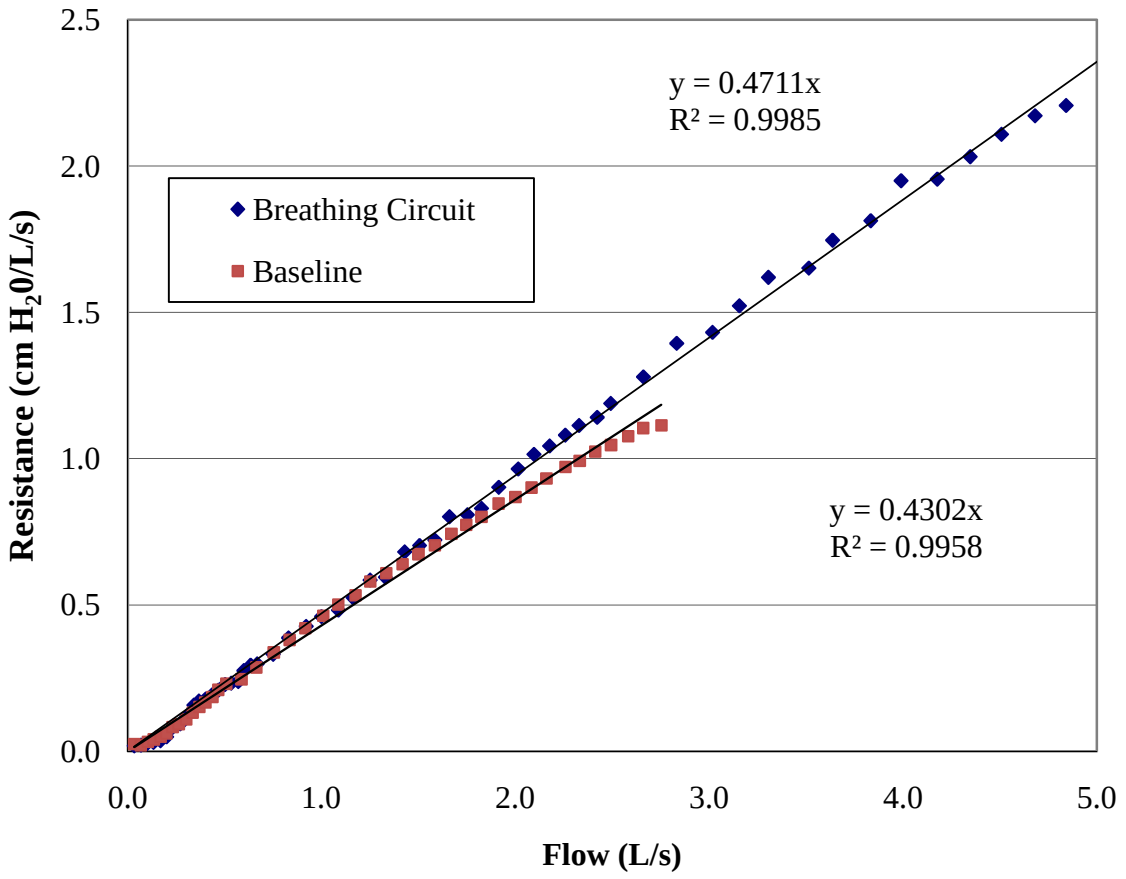


**Figure 2.14** Resistance to flow given in cm $H_2O$/L/s for the modified breathing circuit and the baseline. At 6.67 L/s (400 L/min) the resistance to flow is 3.14 cm $H_20$/L/s for the modified breathing circuit versus 2.87 cm $H_20$/L/s for the baseline pressure housing.

**Table 2.1** Three basic sensors used in each series of prototype designs with a description of the modifications

| Basic Sensors | Sensor ID | Description of Modification | Extension (mm) | Circ. (mm) (D$\pi$)** |
|---|---|---|---|---|
| **Sensor #1** - Standard sensor with no modifications* | 1A | No modification | 17.9 | 48.0 |
| | 1B | Flow orifice completely covered | 17.9 | 48.0 |
| | 1C | Proximal flow orifice 2/3 covered | 17.9 | 48.0 |
| | 1D | Proximal flow orifice 1/2 covered | 17.9 | 48.0 |
| | 1E | Proximal flow orifice 1/3 | 17.9 | 48.0 |
| | 1F | Distal flow orifice 1/2 covered | 17.9 | 48.0 |
| | 1G | Distal flow orifice 1/3 covered | 17.9 | 48.0 |
| **Sensor #2**- Standard sensor with an 10.7 x 16.9 mm portion cut away 8.4 mm from the base | 2A | No modification | 18.0 | 31.2 |
| | 2B | Flow orifice completely covered | 18.0 | 31.2 |
| | 2C | Distal flow orifice 2/3 covered | 18.0 | 31.2 |
| | 2D | Distal flow orifice 1/2 covered | 18.0 | 31.2 |
| | 2E | Input coupling extended | 24.7 | 31.2 |
| | 2F | Input coupling extended and outer circumference widened | 24.7 | 33.0 |
| **Sensor #3** – Inlet coupling was shortened to 10.1 mm | 3A | No modification | 10.1 | 48.0 |
| | 3B | Input coupling extended and outer circumference widened | 18.6 | 31.3 |
| | 3C | Input coupling extended and outer circumference widened | 18.9 | 25.5 |
| | 3D | Input coupling extended and outer circumference widened | 19.7 | 23.6 |
| | 3E | Input coupling extended and outer circumference widened | 25.4 | 25.3 |

* A standard sensor has an input coupling of 15.3 mm outer diameter and a 13.3 mm inner diameter.

** Remaining distal circumference after a portion of the input coupling had been removed

**Table 2.2** ESPRIT Ventilator Settings

| | | |
|---|---|---|
| **TV** | 1037 | mL |
| **TR** | 10 | BPM |
| **Total VE** | 10.4 | L |
| **PIP** | 44.3 | cm $H_20$ |
| **Rate** | 10 | BPM |
| **$O_2$** | 21% | |

**Table 2.3** The $ETCO_2$ (mmHg) and error for Sensor #1 and its modifications

| | **Ref** | **Test** | **Ref** | **% Error** |
|---|---|---|---|---|
| 1A | 35.0 | - | 35.0 | |
| 1B | 36.7 | 36.2 | 36.6 | -1.20% |
| 1C | 36.5 | 35.9 | 36.6 | -1.64% |
| 1D | 36.4 | 35.6 | 36.3 | -2.12% |
| 1E | 35.4 | - | 35.3 | |
| 1F | 36.2 | 36.6 | 36.4 | 0.88% |
| 1G | 36.3 | 37.1 | 36.3 | 2.23% |

**Table 2.4** The $ETCO_2$ (mmHg) and error for Sensor #2 and its modifications

| | **Ref** | **Test** | **Ref** | **% Error** |
|---|---|---|---|---|
| 2A | 35.4 | 31.6 | 35.4 | -10.73% |
| 2B | 36.4 | 36.5 | 36.4 | 0.27% |
| 2C | 36.0 | 36.2 | 35.9 | 0.70% |
| 2D | 35.9 | 36.0 | 35.9 | 0.28% |
| 2E | 36.2 | 35.7 | 36.3 | -1.63% |
| 2F | 36.2 | 35.3 | 36.3 | -2.59% |

**Table2.5** The $ETCO_2$ (mmHg) and error for Sensor #3 and its modifications

| | **Ref** | **Test** | **Ref** | **% Error** |
|---|---|---|---|---|
| 3A | 35.9 | | 36.0 | |
| 3B | 35.7 | 33.7 | 35.7 | - 5.60% |
| 3C | 35.8 | 35.2 | 35.8 | - 1.68% |
| 3D | 35.9 | 34.7 | 35.9 | - 3.34% |
| 3E | 35.9 | 35.4 | 35.9 | - 1.39% |

# CHAPTER 3

# CALIBRATION OF THE DIFFENTIAL PRESSURE FLOW SENSOR

## 3.1. Introduction

Flow sensing devices, known as pneumotachometers, are devices that measure gas flow based on a transducer signal that is integrated over time to produce volume. When a flat plate with a small opening is inserted into the pipe perpendicular to the flow, the restricted opening causes a pressure drop. The obstacle created by the orifice causes the fluid particles to collide with each other, converting the velocity into heat and pressure. The added pressure increases the velocity of the particles passing through the orifice opening. Once through the opening the pressure is released. Pressure taps before and after the orifice plate measure the differential pressure drop. A resistive unit within the sensor produces a signal proportional to the pressure drop. Based on the Bernoulli equation, the flow rate is roughly proportional to the square root of the differential pressure.

Nonlinear differential pressure sensors calculate flow indirectly; therefore, a discharge correction factor is necessary to adjust the flow calculations to correct for head loses and turbulent flow. This correction factor is dependent on many factors including the Reynolds number, sensing tap locations, length of the orifice, and orifice diameter. Therefore, the discharge coefficient is specific to each individual sensor design.

Calculation of the discharge coefficient is well defined in the literature and is recommended for precise measurements of flow.[33-35] The differential pressure was recorded across a wide range of volumetric flows and stores in a lookup table. The table, indexed by the Reynolds number, is then incorporated into the software algorithms. The accuracy of the flow measurements with the adjustment of the discharge coefficient verses the actual recorded flow are also reported.

## 3.2. Materials and Methods

### 3.2.1. Experimental Design

The following experimental setup was used to characterize flow across the sensor, **Figure 3.1.** Constant air flow at ambient conditions was provided by an ESPRIT Ventilator (Phillips-Respironics, Carlsbad, California). The ventilator was connected to the high flow input on a VT Plus Gas Flow Analyzer (Bio-Tek, Winooski, Vermont). This served the purpose of verifying the flow rate setting selected on the ventilator. The VT Plus was calibrated using a 3 liter syringe and found to be within ±1.60%. The flow sensor was connected to the high flow exhaust on the VT Plus. The sensor was connected to the FloTrac Elite and then to a laptop. NICO Data collection software recorded the oxygen, carbon dioxide, and differential pressure signals. The average flow ranged from 2-300 L/min.

### 3.2.2. Analysis - Theory of Discharge Coefficient

The Bernoulli equation is used to relate differential pressure and velocity to volumetric flow. An overview of the derivation is provided below. An in depth

description can be found in fluid mechanics textbooks.[36,37] The following parameters are commonly used to describe gas flow:

| | | |
|---|---|---|
| A | Effective cross-sectional area | ($m^2$) |
| v | Velocity | ($m/s^2$) |
| ρ | Density | ($kg/m^3$) |
| P | Absolute Pressure | ($N/m^2$) |
| Q | Volumetric Flow | ($m^3/s$) |

The subscript "1" and "2" will denote the parameter correlates to the pressure tap located upstream and downstream of the pressure tap, respectively.

By assuming a horizontal flow and minimal viscosity, the Bernoulli Equation is used to determine conservation of energy between the upstream and downstream pressure taps:

$$P_1 + \frac{1}{2}\rho v_1^2 = P_2 + \frac{1}{2}\rho v_2^2 \qquad [3.1]$$

By rearranging the terms, the equation can be written in terms of the differential pressure.

$$\Delta P = P_1 - P_2 = \frac{\rho}{2}(v_2^2 - v_1^2) \qquad [3.2]$$

Assuming constant density, the relationship between volumetric flow, area, and velocity is given by the Equation of Continuity.

$$Q = A_1 v_1 = A_2 v_2 \qquad [3.3]$$

Solving **Equation 3.3** for $v_1$ and substituting it into **Equation 3.2** yields:

$$\Delta P = \frac{\rho}{2}\left( v_2^2 - \left( \frac{(A_2 v_2)^2}{A_1} \right) \right) = \frac{\rho}{2}\left( 1 - \left( \frac{A_2}{A_1} \right)^2 \right) v_2^2 \qquad [3.4]$$

where ΔP is the measured differential pressure.

To solve for the volumetric flow, **Equation 3.4** is written in terms of $v_2$ and the equation becomes

$$Q_i = A_2 v_2 = A_2 \sqrt{\frac{2\Delta P}{\rho\left( 1 - \frac{A_2^2}{A_1^2} \right)}} = \sqrt{2\left( \frac{A_1^2 A_2^2}{A_1^2 - A_2^2} \right)\frac{\Delta P}{\rho}} \qquad [3.5]$$

where $Q_i$ is the ideal flow. To reduce the number of terms in the equation, a constant of proportionality introduced

$$Q_i = K\sqrt{\frac{\Delta P}{\rho}} \qquad [3.6]$$

where K has units of square meters.

3.2.2.1. Introduction of temperature and pressure terms. The properties of a particular gas are dependent on the pressure, volume, and temperature, ideally given by the equation

$$PV = nZRT \quad [3.7]$$

where P is the absolute pressure ($N/m^2$), V is the volume ($m^3$), T is the temperature in Kelvin (K) n is the amount of the gas (mol), Z is a dimensionless compressibility factor, and R is the universal gas constant (N m/mol K).

The number of moles in a gas can be expressed in terms of the molar mass and the mass

$$n = \frac{m}{M_m} \quad [3.8]$$

where m is the mass in kg and $M_m$ is the molar mass in kg/mol.

The density of a fixed volume of gas with a known mass is given by **Equation 3.9.** The ideal gas law can then be used to introduce the temperature and pressure terms by

$$\rho = \frac{m}{V} = \frac{M_m P}{ZRT} \quad [3.9]$$

The volumetric flow equation, with the added pressure and temperature terms from **Equation 3.9,** then becomes

$$Q = K\sqrt{\frac{\Delta PZRT}{M_m P}} \qquad [3.10]$$

3.2.2.2. Correcting to base conditions. In order to correct the measured flow to standard conditions a method for utilizing the ideal gas law was developed. Briefly

$$nR = \frac{P_{stp}V_{stp}}{Z_{stp}T_{stp}} \qquad [3.11]$$

$$nR = \frac{P_f V_f}{Z_f T_f} \qquad [3.12]$$

where the subscript “stp” is used to designate standard temperature and pressure conditions and “f” refers to the measured conditions of the flowing gas. By setting the equations equal to each other and differentiating both sides with respect to time, the volume term becomes volumetric flow so that

$$\frac{P_{stp}Q_{st}}{Z_{stp}T_{stp}} = \frac{P_f Q_f}{Z_f T_f} \qquad [3.13]$$

where $Q_{stp}$ and $Q_f$ are the volumetric flow rates of the gas relative to the standard temperature and pressure at sea level and the conditions where the flowing gas was measured , respectively. Solving Equation 1.13 for $Q_{stp}$ gives

$$Q_{stp} = \frac{P_f T_{stp} Z_{stp}}{P_{stp} T_f Z_f} Q_f \qquad [3.14]$$

To convert **Equation 3.10** from the flowing conditions to standard conditions it is combined with **Equation 3.14**

$$Q_{stp} = \frac{P_f T_{stp} Z_{stp}}{P_{stp} T_f Z_f} K \sqrt{\frac{\Delta P Z_f R T_f}{M_m P_f}} \qquad [3.15]$$

K will absorbs the constant terms as before so that

$$K = \frac{Z_{stp}}{Z_f} \sqrt{2\left(\frac{A_1^2 A_2^2}{A_1^2 - A_2^2}\right) Z_f R} \qquad [3.16]$$

The units of K now become

$$K \cdot units = \sqrt{\frac{N \cdot m}{mol \cdot K}^5} \qquad [3.17]$$

And the final equation to convert the volumetric flow $Q_f$ to standard conditions $Q_{stp}$ is given by

$$Q_{stp} = \frac{P_f T_{stp}}{P_{stp} T_f} K \sqrt{\frac{\Delta P T_f}{M_m P_f}} \qquad [3.18]$$

where the units cancel

$$\frac{m^3}{s} = \frac{Pa \cdot K}{Pa \cdot K} \sqrt{\frac{N \cdot m}{mol \cdot K}^5} \cdot \sqrt{\frac{Pa \cdot K}{\left(\frac{kg}{mol}\right) \cdot Pa}} = \sqrt{\frac{kg \cdot m}{kg \cdot s^2}^6} = \sqrt{\frac{m^6}{s^2}} \qquad [3.19]$$

such that the units of flow is given in $m^3/s$.

3.2.2.3. Determining discharge coefficient. A main assumption of the Bernoulli equation is that no head loss occurs between points (1) and (2), as shown in **Figure 3.2**. Therefore, it is necessary to include an empirical coefficient to correct for the difference between the actual flow rate and the ideal flow rate. Introducing the constant is advantageous because it allows for the correction of errors that may arise due to changes in gas velocity composition. The constant, when indexed by the Reynolds number, can also be used to correct for variations in dynamic viscosity. This constant, known as a discharge coefficient $C_d$, is a function of the orifice opening.

Ideally, the flow through the orifice would be given by the equation

$$Q_i = A_i \upsilon_i \qquad [3.20]$$

where $Q_i$ is the ideal volumetric flow, $A_i$ is the ideal area which is equivalent to the orifice opening $A_o$, and $v_i$ is the ideal gas flow. Ideal velocity is computed by the Bernoulli equation.

However, the flow of gas through an orifice is such that the minimum cross-sectional area of the jet $A_2$ is always smaller than that of the orifice $A_0$. The velocity profile through the orifice is not uniform, which leads to a point at $A_2$ known as the vena contracta. At this point the velocity is at its highest due to converging streamlines. Due to the complex flow profile, it is difficult to measure the value of $A_2$ at the vena contracta. Head losses associated with turbulent flow caused by the orifice plate also make it impossible to calculate true flow theoretically. The discharge coefficient relates the actual flow to the ideal flow:

$$C_d = \frac{ActualFlow}{IdealFlow} \qquad [3.21]$$

so that

$$Q = C_d Q_i \qquad [3.22]$$

By this definition the discharge coefficient is an integer that 0 to 1.

The flow discharge is highly dependent on orifice geometry and the Reynolds number. The Reynolds number, a unit-less dimension used to characterize laminar or turbulent conditions, is given by

$$\mathrm{Re} = \frac{\upsilon D \rho}{\mu} \qquad [3.23]$$

where

| | | |
|---|---|---|
| ν | velocity | (m/s) |
| μ | dynamic viscosity | (Pa s or N s/$m^2$) |
| ρ | density | ($kg/m^3$) |
| D | diameter of Pipe | (m) |

Using the relationship established in **Equation 3.9** for density, the Reynolds number becomes

$$\mathrm{Re} = \frac{\upsilon D M_m P_f}{\mu Z R T_f} \qquad [3.24]$$

where $M_m$ is the molecular mass, $P_f$ and $T_f$ refer to the pressure and temperature of the flowing gas, Z is the gas compressibility factor, and R is the universal gas constant. **Equation 3.24** is simplified by combining the constant terms into a constant called "A" as shown

$$A = \frac{D}{ZR} \qquad [3.25]$$

To a first approximation, the velocity term is proportional to the square-root of the differential pressure so the Reynolds numbers becomes

$$\mathrm{Re} = A\sqrt{\Delta P}\,\frac{M_m P_f}{\mu T_f} \qquad [3.26]$$

For the purpose of this study, the discharge coefficient will be determined experimentally and implemented into the final equation of volumetric flow as a lookup table, which will use the Reynolds number as an index number. When the discharge coefficient was determined experimentally is it combined with the other constant terms in **Equation 3.18**, to give flow coefficient, C. Consequently the coefficient can be greater than one. A weighted average linear interpolation should be applied to determine values not specified in the index table.

## 3.3. Results

### 3.3.1. Discharge Coefficient

The analogue-to-digital (ADC) differential pressure signal was recorded was recorded at incremental flow rates from 0 to 300 liters/minute, the maximum flow that could be obtained with the ventilator. For discharge coefficient analysis the ADC signal was converted into SI units of pressure. Pressure and temperature of the flowing gas were measured at 84.5 kPa and 297.5 K, respectively. The molecular mass of air was defined as 0.028669 kg/mol. According to the National Institute of Standards Technology, a standard pressure of $P_{stp}$ = 101.325 kPa and temperature of $T_{stp}$ = 293.15 K were used in the calculations.

Due to the experimental design, the discharge coefficient was combined with the constant of proportionality term given in **Equation 3.6**. For convenience, this term will be referred to as the flow discharge coefficient, C. Rearranging the terms of Equation 3.18, the discharge coefficient at a given flow becomes

$$C = \frac{\frac{P_f T_{stp}}{P_{stp} T_f}\sqrt{\frac{\Delta P T_f}{M_m P_f}}}{Q_{stp}} \qquad [3.27]$$

Because coefficient C takes into account factors including the cross-sectional area and fluid viscosity, it will not be an integer from 0 to 1.

To create a flow coefficient lookup table, the flow coefficient was indexed by the Reynolds number. The Reynolds number given in Equation 3.26 includes a constant term, A, which includes the diameter, gas compressibility factor, and universal gas constant. The nature of the prototype was such that a specific diameter of the breathing circuit was not defined. Instead, the constant was set equal to one. The Reynolds number reported is therefore scaled. This shall be denoted by the prime symbol following the Reynolds number, R'.

The flow coefficient as indexed by a scaled Reynolds number is given in **Figure 3.3.** During laminar flow (low Reynolds numbers) there is a sharp spike seen in the flow coefficient. As the Reynolds number increases the flow coefficient stabilizes around 30.5.

For the index table that would be incorporated into the flow algorithms the flow coefficient values were weighted. The measured volumetric flow was more dependent on

the flow coefficient at low Reynolds numbers than at high ones. For an R' < 2,300,000, an average of ±1 data point to the right and the left of the flow coefficient was taken, for a total of n = 3 data points. Above R' >= 2,300,000 the flow coefficient remained stable and was set at a constant value of 30.4822.

The index table is given in **Table 3.1**. **Figure 3.4** is a graphical representation of the weighted flow coefficients. For values not specified on the table, a linear interpolation between the two nearest integers should be applied. For example, if an index of 1,500,000 was returned, the flow coefficient would be a weight average of the index points of 1,438,328 and 1,559,968.

To test the accuracy of the sensor using the modified discharge coefficient, the calculated volumetric flow was compared to the recorded volumetric flow. For an R>=650,000 to be within 3%; for R<650,000 the sensor was accurate to within ±0.8 liter.

## 3.4. Discussion

The purpose of this effort was to calibrate the prototype flow sensor by determining the discharge coefficient. Orifice plates are commonly used to measure the flow of natural gases. The need for a discharge coefficient to account for head losses and changes in area that cannot be calculated theoretically has been recognized. When the orifice opening is circular, guidelines set forth by the International Organization of Standards (ISO) detail the process for determining the discharge coefficient based on empirical equations (ISO 5167-1).[38,39]

Ideally, the flow rate could also be calculated experimentally using **Equation 3.20**, but because the original sensor was designed for exercise applications the orifice

opening is not a perfect circle. Instead it includes conduit for saliva and moisture, **Figure 3.5,** which accumulates when breathing through a mask**.** Moisture buildup along the inner wall of the sensor around the orifice ring can effectively change the sensor geometry. So, while it is necessary to prevent the buildup of fluids within the sensor housing, it makes the area of the actual orifice opening difficult to calculate theoretically.

The Reynolds number is a dimensional number that is used as a way to quantify the effects of the inertial and viscous forces within a fluid. When the viscosity forces are predominant the fluids profiles is streamline. This is known as laminar flow and is characterized by a constant fluid motion, minimal disruptions, and a Reynolds number less than 2,300. When the Reynolds number is above 2,300 the flow is turbulent. The inertial forces become more prevalent and the flow experiences random eddies and other disturbances. Because the Reynolds number in this study was scaled, the transition from laminar to turbulent flow does not occur at R=2,300.

The flow coefficient for the prototype sensor revealed a sharp spike at low flows, followed by a transition period, and then the flow coefficient stabilized. This pattern was observed in several independent trials. In their studies of small sharp-edged cylindrical orifices, Ramamurthi et al (1999) found that at low Reynolds numbers the flow profile varied based on the aspect ratio of the length to the diameter of the orifice (*l/d*). They suspect the spike in discharge coefficient could be a result of added pressure due to the surface tension of water. When the Reynolds number is high, the surface tension induced pressures are negligible. The discharge coefficient is no longer dependent on the flow profile (i.e., Reynolds number).[40-42]

As seen in the derivation, the flow coefficient is highly sensitive to changes in the geometry of the orifice and flow profiles. One limitation of this study was the flow sensor calibration was based on a single prototype system. Before the system could be sold commercially several prototype systems with the exact same specifications would be manufactured. Each individual system could be calibrated. To improve the accuracy of the flow coefficient, each individual system could be calibrated and the results reported as a composite flow coefficient table.

Another limitation of the experimental design was the sensor was tested under constant airflow. During a practical application, the sensor will be subjected to various expired flow rates as the individual breaths in and out. At low flows the resolution of the signal decreases, but at high flows the signal strength is high. During a normal breath this could be problematic since the flow during the exhale breath is drawn out. However, during exercise the transition of flow from an inhale to and exhale happens rapidly and there is a minimal amount of time spent while flow is low.

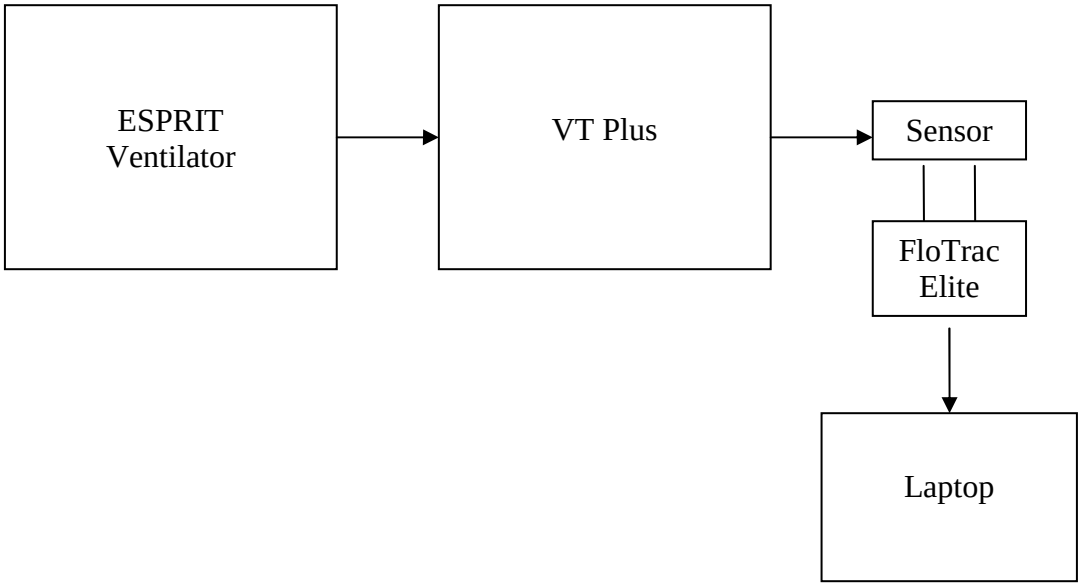


**Figure 3.1** Experimental setup for flow calibration

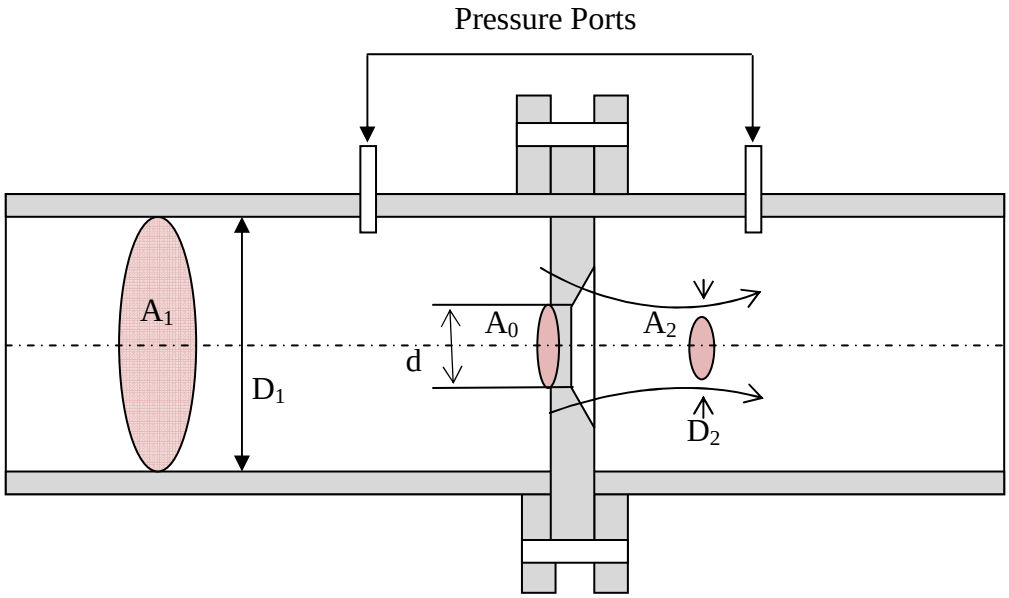


**Figure 3.2** To create a pressure drop an obstruction is placed in the middle of the two pressure ports. The area at the vena contracta, A2, is always smaller than A0. Because the area at A2 is difficult to measure, the discharge coefficient is used to relate the difference in the actual and ideal flow.

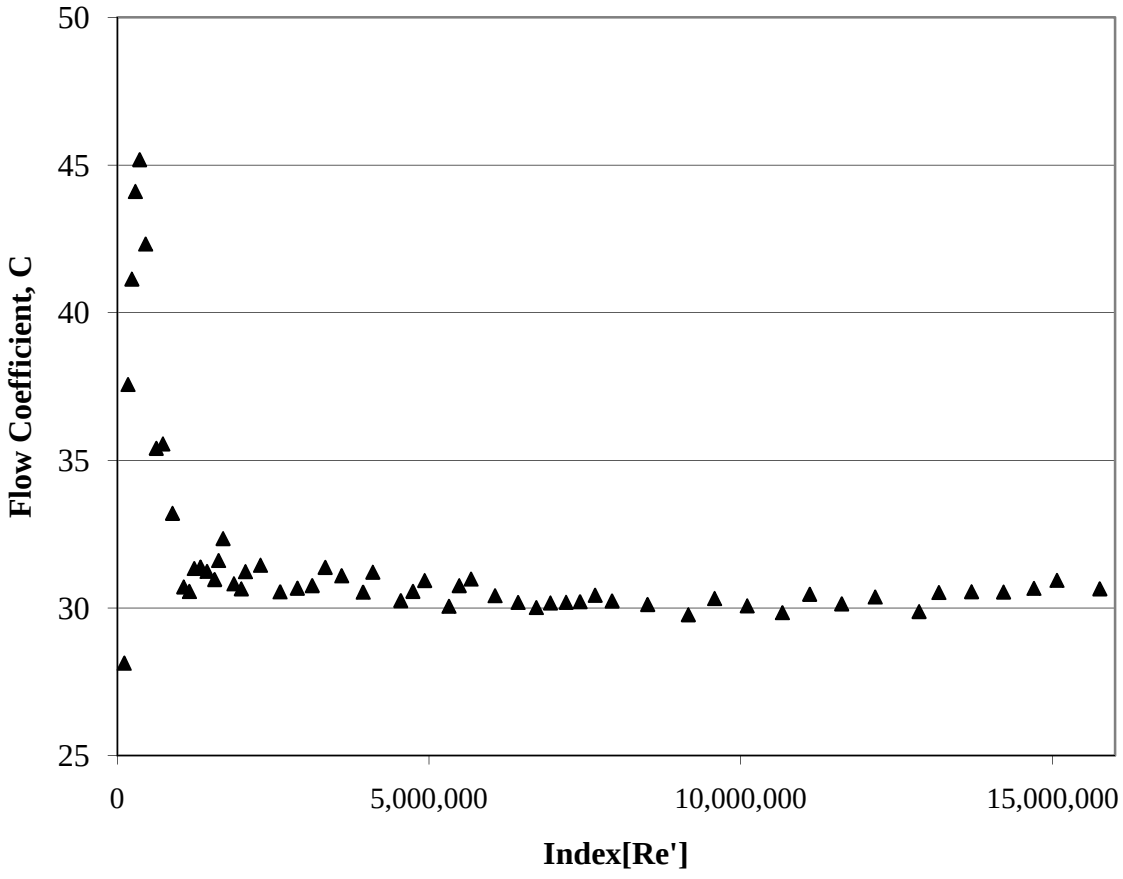


**Figure 3.3** The flow coefficient C, which includes the discharge coefficient $C_d$ and the constant of proportionality K, indexed by a scaled Reynolds number

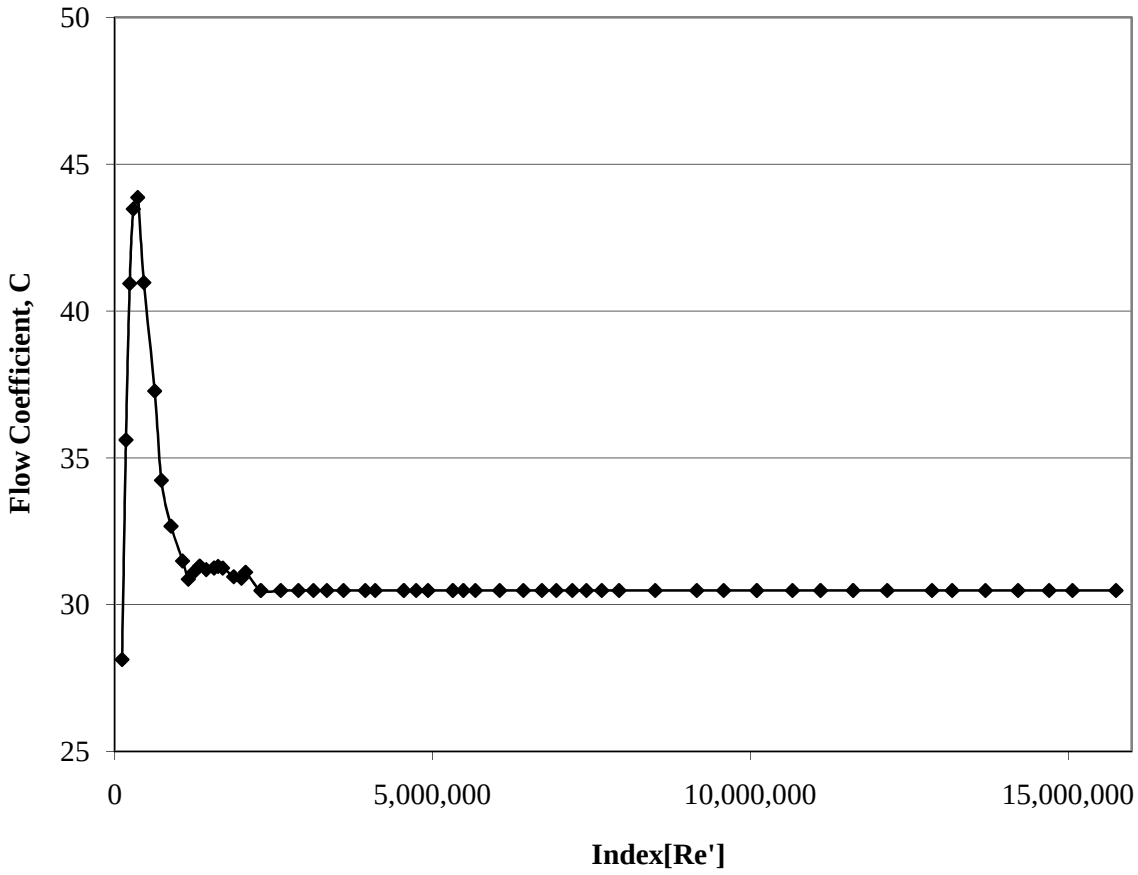


**Figure 3.4** The weighted flow coefficient as it would be referred to in the software algorithms

**Figure 3.5** End view of the differential pressure orifice opening**.**

**Table 3.1** The flow coefficient table indexed by a scaled Reynolds number

| R' | C |
|---|---|
| 111804 | 28.1311 |
| 172569 | 35.6126 |
| 232476 | 40.9369 |
| 288890 | 43.4748 |
| 358718 | 43.8701 |
| 454960 | 40.9708 |
| 625447 | 37.2761 |
| 731142 | 34.2370 |
| 884307 | 32.6726 |
| 1065856 | 31.4932 |
| 1155241 | 30.8690 |
| 1234175 | 31.0938 |
| 1334371 | 31.3202 |
| 1438328 | 31.1962 |
| 1559968 | 31.2520 |
| 1624618 | 31.3012 |
| 1696356 | 31.2526 |
| 1869371 | 30.9505 |
| 1989604 | 30.8983 |
| 2055320 | 31.1084 |
| >2300000 | 30.4822 |

# CHAPTER 4

# VALIDATION OF LUMINESCENCE QUENCHING OXYGEN SENSOR

## 4.1. Introduction

In vitro testing of oxygen uptake during exercise was performed using a propane combustion patient lung simulator. The ratio of the rate of carbon dioxide production per minute ($VCO_2$) over the rate of oxygen consumption per minute ($VO_2$) is known as the respiratory quotient (RQ). When burned completely, the combustion of propane to form carbon dioxide and water vapor has a standard RQ of 0.6. This method is often used to check the accuracy of $VO_2$ and $VCO_2$ measurements for metabolic monitors.[43,44]

In previous bench testing of the oxygen uptake measurements for clinical use, the oxygen sensor was found to be accurate to within 0.3±2.8% of the measured oxygen. When compared with the clinical gold standard device (Deltatrac, Datex, Helsinki, Finland) the error in the oxygen consumption of 2.2±4.1% was found to be well within an acceptable range for clinical use. The system was again tested on 14 intensive care unit patients and found to be within 1.7±6.9% of the reference analyzer.

Oxygen consumption will be determined theoretically and then compared to the measurements recorded during the propane simulation with constant air flow. To be suitable for an exercise application, the oxygen sensor measurement should be accurate to within ±5% of the measured fraction of expired oxygen.

## 4.2. Materials and Methods

### 4.2.1. Experimental Design

The propane lung simulator setup is shown in **Figure 4.1**. A propane burner was mounted inside a glass chamber with inlet and outlet flows. The inlet flow was connected to an ESRIT Ventilator (Phillips-Respironics, Carlsbad, California), which provided the oxygen necessary for combustion. The rate of inspired air $V_I$ (L/min) was measured using the VT Plus Gas Flow Analyzer (Bio-Tek, Winooski, Vermont) before it entered the chamber. The differential pressure and oxygen sensors provided on-airway analysis of the gas as it exited the chamber in the outlet flow.

The burner was connected to a flow rotometer with a needle valve (NV). The arbitrary settings on the needle valve controlled the propane flow rate. To keep the system cool and prevent damage to the parts, cold water was circulated in coils within the glass chamber.

The oxygen and differential pressure sensors were connected to a FloTrac Elite (Phillips-Respironics, Carlsbad, California), which used algorithms to determine the fraction of expired oxygen and gas flow. The FloTrac Elite was connected to a laptop, which recorded the various parameters including fraction of expired carbon dioxide ($FeCO_2$), the fraction of expired oxygen ($FeO_2$), and flow signals.

### 4.2.2. Calibration Curve

It was first necessary to create a calibration curve relating the amount of propane burned (i.e., the NV placement on the flow rotometer) with the oxygen consumed. The propane tank was placed on a scale and the mass in grams was recorded. A scale

recorded the mass of propane burned at four settings (15, 20, 25, and 30) on the needle valve. The propane NV was held constant while the air flow from the ventilator was varied. Air flows of approximately 10, 15, 25, 40, and 60 L/min were selected. At each setting measurements were taken every 3 minutes for 9 minutes. The rate of propane consumption was dependent on the NV placement and did not vary across the air flow rates. The average propane mass loss for 45 minutes was reported in the calibration curve.

When oxygen is not a limiting factor, the molecular formula for complete propane combustion is given by

$$C_3H_8 \text{ (propane)} + 5\ O_2 \rightarrow 3\ CO_2 + 4\ H_2O + \text{heat} \qquad [4.1]$$

The amount of propane consumed in grams/min was converted to mol/min using the molecular weight of propane. Five moles of oxygen are consumed for every one mole of propane. The ideal gas law was used to determine the number of ml/min of $O_2$ consumed at ambient conditions. At standard conditions one mole of gas occupies 22.4 liters.

### 4.2.3. Validation of $O_2$ Sensor During Simulated Exercise

The accuracy of the oxygen sensor was tested at four propane combustions levels, which corresponded to the needle valve placement at 15, 20, 25 and 30. At ambient conditions, the $VO_2$ at these levels was determined in the calibration to be approximately 323, 430, 538, and 646 ml/min, respectively.

The same NV and flow rate settings were used for the $O_2$ sensor validation as in the calibration curve. A stabilization period of 5 minutes was allowed in between each NV setting. Then the $V_I$, $FeO_2$, $FeCO_2$, and differential pressure were all recorded every 3 minutes for 9 minutes total at each flow increment and the average was reported. Relative humidity and temperature of the inspired and expired gas were monitored using an Omega RH81 Thermo Hydrometer (Omega, Stamford, Connecticut).

4.2.4. Relative Humidity Correction

Dry air is a composite of 78.8% nitrogen, 20.9% oxygen, 0.9% argon, and 0.03% carbon dioxide. However, for most practical applications there is also 1-3% water vapor present, so it was necessary to adjust the composition percentages accordingly.

Relative humidity (RH) is the ratio of the actual partial pressure of water vapor in ambient conditions and the saturation pressure of water at the ambient temperature

$$\%RH = \frac{p_v}{p_{sat}} \qquad [4.2]$$

where RH is the relative humidity, $p_v$ is the partial pressure of water vapor, and $p_{sat}$ is the saturation pressure of water at the ambient temperature. The saturation pressure of water at a given temperature is derived empirically where

$$p_{sat} = 6.1078 * 10 \exp\left(\frac{7.5T - 2048.65}{T - 35.85}\right) \qquad [4.3]$$

where T is the temperature in Kelvin.

Water vapor changes the fraction of inspired gases so that

$$F_I H_2 O = \frac{p_v}{p_{bar}} \quad [4.4]$$

and

$$F_I O_2 = \frac{p_{bar} - p_v}{p_{bar}} * 0.2093 \quad [4.5]$$

For the purposes of this study the fraction of inspired argon and carbon dioxide are negligible.

4.2.5. Analysis of Calculated $FeO_2$

The rate of oxygen consumption ($VO_2$) is the difference between the volumes of inspired air ($V_I$) multiplied by the fraction of inspired oxygen ($F_IO_2$) and the volume of expired air ($V_E$) multiplied by the fraction of expired oxygen ($F_eO_2$) as shown

$$\dot{V}O_2 = \left(\dot{V}_I * F_I O_2\right) - \left(\dot{V}_E * F_E O_2\right) \quad [4.6]$$

$N_2$ is neither used nor produced in metabolism. Therefore, the volume of $N_2$ inhaled must be equal to the volume exhaled according to the Haldane transformation as follows

$$\dot{V}_I \times F_I N_2 = \dot{V}_E \times F_I N_2 \qquad [4.7]$$

where

$$F_I N_2 = 1 - F_I O_2 - F_I CO_2 - F_I H_2 O \qquad [4.8]$$

$$F_E N_2 = 1 - F_E O_2 - F_E CO_2 - F_E H_2 O \qquad [4.9]$$

It follows that by substituting **Equations 4.8** and **4.9** into **Equation 4.7** and rearranging the terms the equation becomes

$$\dot{V}_E = \dot{V}_I \frac{F_{I\,N_2}}{F_{EN_2}} = \left( \frac{\left(1 - F_I O_2 - F_I CO_2 - F_I H_2 O\right)}{\left(1 - F_E O_2 - F_E CO_2 - F_E H_2 O\right)} \right) \dot{V}_I \qquad [4.10]$$

Using this relationship to eliminate $V_E$ the theoretical $F_EO_2$ at the ambient conditions is determined by

$$\dot{V}O_2 = \left(\dot{V}_I * F_I O_2\right) - \left( \frac{\left(1 - F_I O_2 - F_I CO_2 - F_I H_2 O\right)}{\left(1 - F_E O_2 - F_E CO_2 - F_E H_2 O\right)} \right) \dot{V}_I * F_E O_2 \qquad [4.11]$$

By simplifying the equation and assuming minimal carbon dioxide in the air (i.e. $F_ICO_2$ = 0) the equation yields

$$\frac{\dot{V}O_2}{\dot{V}_I} = F_I O_2 - \left( \frac{(1 - F_I O_2 - F_I H_2 O)}{(1 - F_E O_2 - F_E CO_2 - F_E H_2 O)} \right) F_E O_2 \qquad [4.12]$$

The known parameters included $V_{I,}$ which was recorded by the VT Plus; $VO_{2;}$ which was calculated from the calibration curve; and $FiO_2$, $FiH_20$, $FeCO_2$, and $FeH_20$, which were adjusted based on the relative humidity at ambient conditions. After applying the known parameters into Equation 4.12**,** it was a straightforward process to isolate and solve for the calculated value of $FeO_2$.

## 4.3. Results

### 4.3.1. Calibration Curve

The results of the calibration curve are shown in **Table 4.1.** The total mass loss from the propane combustion at each needle valve setting is shown in the first column. The molecular weight of propane was used to calculate the number of moles burned. Using the ambient conditions and the ideal gas law, the volume in ml/min of oxygen at each needle valve setting was determined in column four. At standard conditions one mole of gas occupies 22.4 liters, as shown in the last column. At ambient conditions, the volume of oxygen consumed (ml/min) was equivalent to 21.544 ($R^2$=0.9998) times the needle valve placement, **Figure 4.2.**

### 4.3.2. Recorded Parameters

At the ambient conditions measured in the lab, the temperature and relative humidity of the inspired air were T = 304.5 K and a RH = 23.1%. The barometric pressure was recorded at $P_{bar}$ = 635 mm Hg. When adjusted for the relative humidity, the

fractions of inspired air are as follows $FiO_2$ = 0.206602, $FiCO_2$ = 0, and $FiH_2O$ = 0.012891.

The results of the propane combustion simulation are given in **Table 4.2.** Two data points are marked with an asterisk. At 10 L/min and a NV = 30 the flame would not stay lit and no measured parameters were reported. This was most likely caused by the large propane consumption being limited by available oxygen in the low flow. At 60 L/min and a NV = 15 the $V_I$ is lower than at the other flows (~50 L/min instead of ~60 L/min). Although the $FiO_2$ and percent error are reported for this value, it is important to take the decrease in $V_I$ into consideration.

4.3.3. Oxygen Validation Measurements and Percent Error

The recorded $FeO_2$ by the oxygen sensor is given in **Table 4.3**. From the calibration curve, the $VO_2$ at each needle valve setting (which relates to the flow of propane controlled by the rotometer) was determined. Going down the columns for a given flow rate, the $FeO_2$ measured in the output flow decreased with increasing propane combustion rates (higher NV settings) and $VO_2$. Moving across the rows, when the propane combustion is held constant the $FeO_2$ increases with increasing flow rates. The difference in $FeO_2$ between the NV settings is more pronounced at lower flows. As the flow increases the difference becomes less significant, **Figure 4.3.**

The calculated $FeO_2$ was the method described in Section 4.2.5. A comparison of the calculated $FeO_2$ and the $FeO_2$ recorded by the oxygen sensor is given in **Table 4.4.** The percent of error is greatest at the low flows and decreases as the flow increases for a given propane level. At constant flow the percent error increases as the propane

consumed also increases. As previously noted, the flow at NV = 15 and 60 L/min was lower than the others. While the exact $FeO_2$ could not be measured, the trend remained consistent.

The chamber design required cooling coils to remove heat within the chamber. Circulating water was pumped the water through the coils. Ice was occasionally added to the water to keep the water at 29° C. This had the immediate effect of reducing the relative humidity in the expired gas, and could possibly why the percent error at NV = 20 and 25 L/min (**Table4. 4**) was slightly lower than expected even though the recorded $FeO_2$ (**Table 4.3**) at that point was within the expected range.

## 4.4. Discussion

The in vitro simulation of an exercising individual conducted in a propane burn combustion chamber found the luminescence quenching oxygen sensor to be accurate within ±6% of the expected $FeO_2$ at the ambient conditions across the entire range of flows tested. The accuracy of the sensor improved as the flow rates increased.

The experimental design had a few limitations. First, the simulation of exercise was limited by the size of propane combustion chamber. Flows larger than 60 L/min would extinguish the flame. During maximal exercise, the minute ventilation of an average 40 year old male is about 90 L/min. Athletes at their peak have minute ventilations that can exceed 200 L/min. This chamber size is more representative of the minute volumes a child would require during exercise.

Another limitation related to the chamber size was the allowable flame size for the propane combustion. During exercise, a 40 year old male weighing 75 kg may have a

$VO_2$ max of 40 ml/kg/min or 3000 ml/min. The flame size limited the maximum oxygen consumption to about 640 ml/min. So even though the sensor is accurate to within ±3% at the highest flow rate and $VO_2$ consumption level tested, the accuracy of the oxygen sensor at higher $VO_2$ levels and flow rates could not be determined.

Relative humidity can also cause errors in the reported oxygen consumption. Relative humidity of the expired gas was measured and the gas analysis was adjusted accordingly. At low air flow rates the expired gas was nearly 100% saturated. However, as the flow rate increased the water concentration in the expired air was diluted. The relative humidity at 60 L/min was around 25%. Air exhaled from the lungs becomes saturated, so this limitation in the experimental design must also be considered.

The most significant limitation is most likely caused by a span error due to the calibration of the oxygen sensor performed by the black box. Span is the variation from the input oxygen and the output oxygen signal. The oxygen sensor is calibrated by zeroing the sensor in room air. As shown in **Figure 4.3**, the expired oxygen signals that were closest to the inspired oxygen signals had lower error than expired oxygen that was farther away from the original value. To reduce the span error the sensor should be zeroed in an additional gas like nitrogen.

Although there were limitations, the purpose of these experiments was to determine if the luminescence-quenching oxygen sensor designed for low flow applications could be expanded to include elevated volumetric air flows. During exercise both flow rates and oxygen consumption levels increase, so it is reasonable to conclude that the $FeO_2$ measured would still be within the limits of sensitivity for the oxygen sensor.

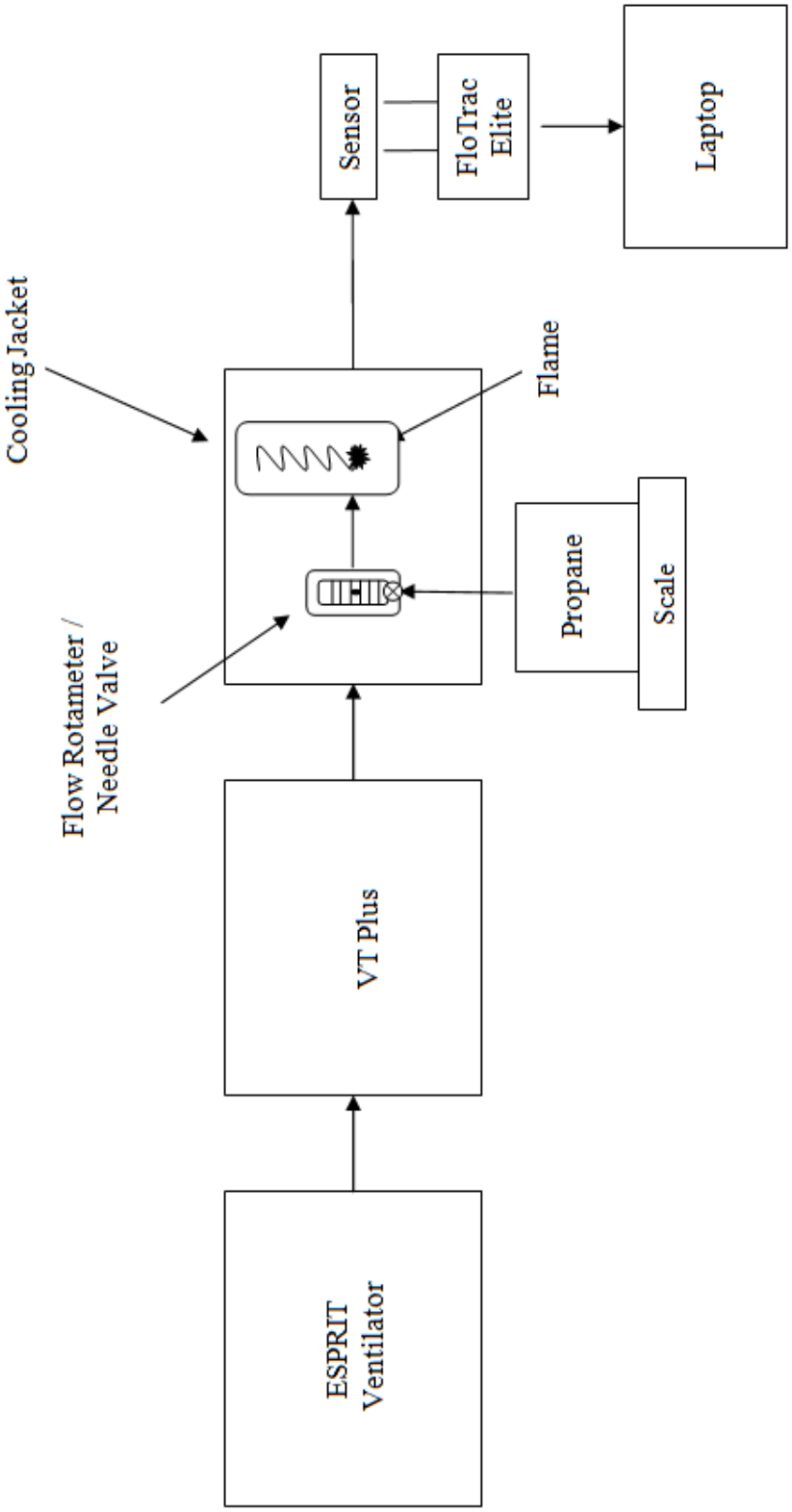


**Figure 4.2** Schematic of Propane Burn Setup

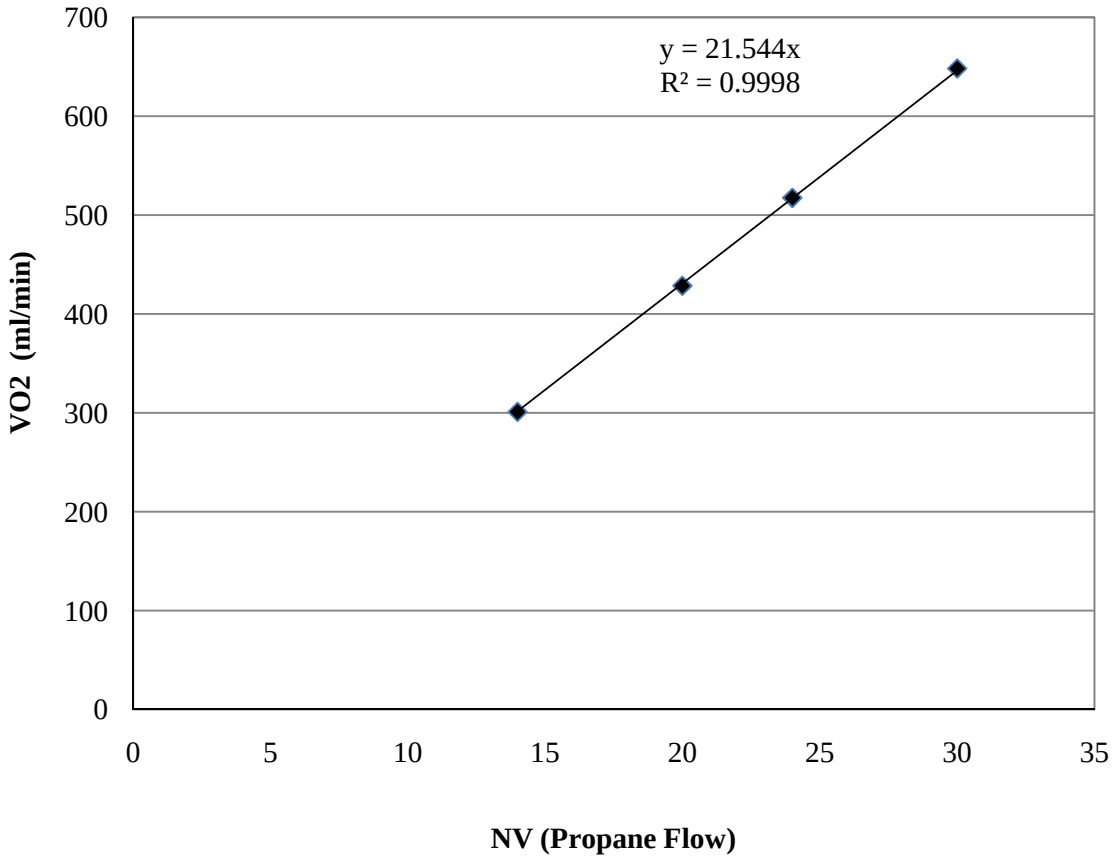


**Figure 4.2** Calibration Curve at Ambient Conditions. The rotometer NV setting controls the rate of propane consumption. The NV setting as it relates to the flow of propane in g/min is given in **Table 4.1**.

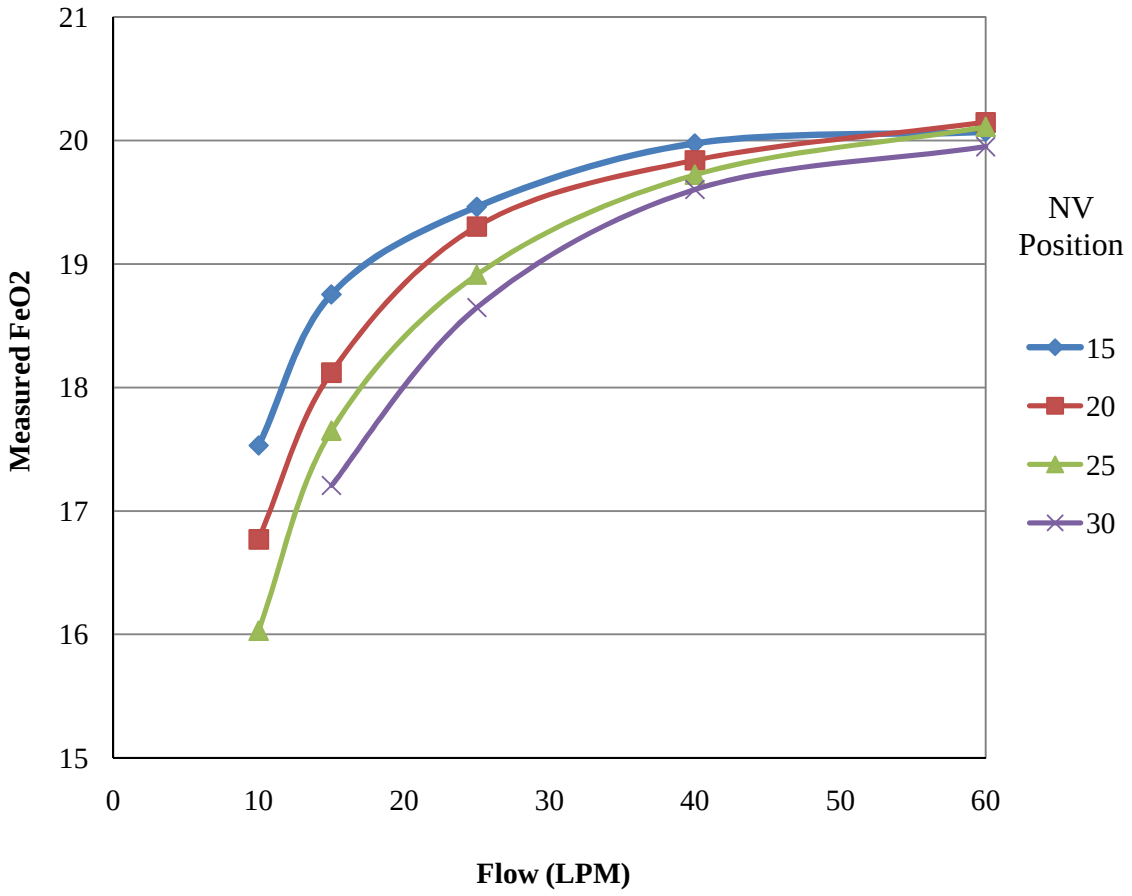


**Figure 4.3** The measured $FeO_2$ recorded by the oxygen sensor for each specific needle valve position, which corresponds to the consumption rate of oxygen. The $FeO_2$ is diluted at high gas flows so there is a minimal difference between the NV settings, but as the flow decreases it is evident that more oxygen is being consumed and hence less remains in the expired gas ($FeO_2$ decreases) at high NV settings.

**Table 4.1** Calibration Curve Conversion

| NV | $C_3H_8$ g/min | $C_3H_8$ mol/min | 5 $VO_2$ mol/min | $VO_2$ ml/min | $VO_2$ STP ml/min |
|---|---|---|---|---|---|
| 15 | 0.095192 | 0.002159 | 0.010793 | 323.1674 | 241.7565 |
| 20 | 0.126922 | 0.002878 | 0.01439 | 430.8899 | 322.342 |
| 25 | 0.158653 | 0.003598 | 0.017988 | 538.6123 | 402.9274 |
| 30 | 0.190383 | 0.004317 | 0.021585 | 646.3348 | 483.5129 |

**Table 4.2** Average (n=3) of $V_I$, $FeO_2$, $FeCO_2$, and $FeH_20$ for the specified NV and flow rate

**10 L/min**

| NV | Flow, $V_I$ | $FeO_2$ | $FeCO_2$ | $FeH_20$ |
|---|---|---|---|---|
| 15 | 9.96 | 0.1753 | 0.0207 | 0.0320 |
| 20 | 10.20 | 0.1677 | 0.0276 | 0.0346 |
| 25 | 9.88 | 0.1603 | 0.0322 | 0.0385 |
| 30* | | | | |

**15 L/min**

| NV | Flow, $V_I$ | $FeO_2$ | $FeCO_2$ | $FeH_20$ |
|---|---|---|---|---|
| 15 | 15.03 | 0.1857 | 0.0140 | 0.0255 |
| 20 | 15.20 | 0.1812 | 0.0186 | 0.0276 |
| 25 | 15.07 | 0.1765 | 0.0227 | 0.0275 |
| 30 | 15.17 | 0.1721 | 0.0260 | 0.0314 |

**25 L/min**

| NV | Flow, $V_I$ | $FeO_2$ | $FeCO_2$ | $FeH_20$ |
|---|---|---|---|---|
| 15 | 24.93 | 0.1946 | 0.0089 | 0.0204 |
| 20 | 24.93 | 0.1903 | 0.0118 | 0.0223 |
| 25 | 24.77 | 0.1891 | 0.0127 | 0.0232 |
| 30 | 25.03 | 0.1865 | 0.0168 | 0.0278 |

**40 L/min**

| NV | Flow, $V_I$ | $FeO_2$ | $FeCO_2$ | $FeH_20$ |
|---|---|---|---|---|
| 15 | 40.23 | 0.1998 | 0.0057 | 0.0153 |
| 20 | 40.13 | 0.1984 | 0.0075 | 0.0185 |
| 25 | 40.00 | 0.1973 | 0.0082 | 0.0185 |
| 30 | 40.57 | 0.1960 | 0.0109 | 0.0227 |

**60 L/min**

| NV | Flow, $V_I$ | $FeO_2$ | $FeCO_2$ | $FeH_20$ |
|---|---|---|---|---|
| 15 | 48.37** | 0.2007 | 0.0048 | 0.0134 |
| 20 | 57.93 | 0.2015 | 0.0055 | 0.0152 |
| 25 | 57.23 | 0.2011 | 0.0066 | 0.0163 |
| 30 | 56.90 | 0.1995 | 0.0082 | 0.0198 |

* Flame would not stay lit at this flow

** Flow did not reach 60 L/min

**Table 4.3** Recorded $FeO_2$ by the luminescence-quenching $O_2$ sensor

| NV | $O_2$ ml/min | 10 L/min | 15 L/min | 25 L/min | 40 L/min | 60 L/min |
|---|---|---|---|---|---|---|
| 15 | 323.2 | 17.53 | 18.57 | 19.46 | 19.98 | 20.07** |
| 20 | 430.88 | 16.77 | 18.12 | 19.03 | 19.84 | 20.15 |
| 25 | 538.6 | 16.03 | 17.65 | 18.91 | 19.73 | 20.11 |
| 30 | 646.32 | * | 17.21 | 18.65 | 19.60 | 19.95 |

* Flame would not stay lit at this flow

** Flow did not reach 60 L/min

**Table 4.4** The percent error between the calculated $FeO_2$ and the recorded $FeO_2$

| NV | $O_2$ ml/min | 10 L/min | 15 L/min | 25 L/min | 40 L/min | 60 L/min |
|---|---|---|---|---|---|---|
| 15 | 323.2 | 1.44% | 0.87% | 0.87% | 0.61% | 0.26%** |
| 20 | 430.88 | 2.81% | 2.18% | 0.93% | 1.54% | 1.20% |
| 25 | 538.6 | 5.77% | 3.47% | 2.45% | 2.19% | 2.05% |
| 30 | 646.32 | * | 5.13% | 3.78% | 3.32% | 2.57% |

* Flame would not stay lit at this flow

** Flow did not reach 60 L/min

# CHAPTER 5

# CONCLUSIONS

## 5.1. Summary of Results

Although there were many limitations of this study, the overall goal was to determine if modifying an existing metabolic system for exercise testing was reasonable. Based on the results presented in this thesis it was concluded that the performance of the prototype system indicates it would indeed be very possible to build such a system. The system applications extend to several large markets and would be profitable. A brief summary of the conclusions for each specific aim presented in this thesis is presented in the following sections. Future work and a few possible applications for luminescence-quenching technology in portable metabolic gas analysis systems is also provided.

### 5.1.1. Prototype Design and Flow Diversion Analysis

The first aim of this study was to build a prototype system with a breathing circuit capable of monitoring exhaled gases flows and concentration during exercise. Flow sensor housing was obtained from a commercially available unit. The gas sensor was inserted into the main lumen of the flow housing at a $90^{o}$ angle creating a T- piece. It was hoped that some air would be diverted from the main flow across the sensor for gas analysis. However, the input coupling of the gas analysis sensor was significantly

narrower than the flow housing exit orifice. The resistance created by the narrowing of the input coupling was too great, and the flow exited through the main flow orifice. To guide flow to the sensor, the extension of the input coupling into the main flow was lengthen and a portion of the input coupling diameter was removed. This acted as a conduit and flow was then diverted to the sensor. The resistance was further minimized when the sensor was inserted at a $45^{o}$ angle into the main lumen.

Through testing of the end-tidal $CO_2$ with this geometry and a reference site, this configuration was selected. The circuit design requires a tradeoff between the resistance to breathing and strength of the differential pressure drop signal. A differential pressure signal of at around 10 cm $H_2O$ at 300 L/min was obtained. The resistance to flow calculated at 400 L/min was around 3.14 cm $H_2O$/L/s for the modified breathing circuit. The resistance was slightly higher than the baseline, a standard differential pressure casing, which had an estimated resistance of 2.81 cm $H_2O$/L/s at the same flow. The prototype system demonstrated strong signal strength at high flows, which was desirable. However, the resistance to flow calculated at high flows was slightly above the recommended values.

So, while modifying the existing breathing circuit allowed for more air flow and improved the signal strength by creating a larger differential pressure drop, it adversely affected the back pressure resistance that a user would experience which could lead to premature gas analysis results. Based on the results, it is reasonable to conclude that with a few more slight modifications the current breathing circuit could be used for exercise stress testing. However, more work is needed to optimize the breathing circuit design.

5.1.2. Flow Sensor Calibration - Discharge Coefficient Table

Flow profiles are subject to specific geometries, therefore, the second aim of this study was to calibrate the flow using the existing sensor configuration. Nonlinear differential pressure flow sensors calculate flow as roughly proportional to the square root of the differential pressure drop. It was necessary to introduce a correction flow coefficient because head losses in the actual flow result in slightly different flow rates than the calculated value. This was achieved by calculating the predicted flow through the orifice and comparing it with the actual measured flow to equate a flow coefficient correction factor that was dependent on the Reynolds number of the flow. With the flow coefficient correction factor, the flow reported by the sensor was accurate to within ±3% or ±1 L. The accuracy of the flow improved with an increasing Reynolds number.

5.1.3. Oxygen Sensor Calibration

The final aim of this research was to calibrate the luminescence quenching oxygen sensor using a propane combustion patient simulator. The oxygen consumption for the complete combustion of propane was calculated theoretically. Then, using the propane simulator which burns propane at a defined rate, the oxygen in the expired gas flow was also measured and used to determine the exact amount of oxygen consumed. The accuracy of the luminescence quenching oxygen sensor was found to be within ±6 % of the measured $FeO_2$ when compared with the theoretical oxygen consumption.

At low levels of propane combustion and air flow the reported accuracy of the oxygen sensor was similar to previous trials. For a given flow the accuracy of the sensor decreased as the oxygen consumption increased, indicating that the flame size was a

limiting factor. The accuracy across the flow range for a given level of oxygen consumption also improved with increasing flow rates. The sensor was most accurate when there was a minimal difference between the fraction of expired oxygen and the concentration of oxygen present for the initial calibration of the system, indicating a span error.

## 5.2. Future Work

The work presented in this thesis was meant to be the first phase in determining the plausibility of constructing a prototype breathing circuit for high flow applications from an existing system used for gas analysis and indirect calorimetry purposes. Before the system could be recommended as an exercise stress analysis instrument, several more phases of research would need to be conducted.

Future work would include building several more prototype breathing circuits. The resistance experienced by the user could be further minimized to fall within the ATS standard for a monitoring device. Although discharge coefficient seems to stabilize at higher flows, the flow could be characterized to ± 400 L/min. Bench testing of the oxygen sensor using a larger propane combustion chamber could model more realistic oxygen consumption levels in an exercising adult. For $VO_2$ max consumption, the levels can reach around 6000 mL/min – well past the scope of the 650 mL/min used for this study.

Another phase of research could include testing other parameters including $VCO_2$ max and sensor performance using a patient lung simulator instead of constant air flow.

The final phase of research would include constructing the actual breathing mask with intake valves. The system then needs to be validated using human volunteers.

## 5.3. Possible Applications

There is currently a strong market for portable metabolic analysis systems. The prototype system is one of the smallest available. It is less than 5 $in^3$ and weighs less than 0.5 Kg total. Moreover, it requires minimal power to operate, is self-calibrating, and user friendly. Given in this section are some possible applications for such a system.

### 5.3.1. Portable Exercise Testing

Portable metabolic monitors are a growing trend in the field of exercise and sports medicine. Athletes and exercise enthusiasts are interested in portable systems to be worn during submaximal workouts as the gas analysis information can be used to guide training programs. Health spas, gyms, personal trainers, and nutritionists advertise gas analysis as a tool for making healthy lifestyle choices. Through a process known as indirect calorimetry, gas analysis can be used to determine an individual's resting metabolic rate (RMR). Because this value accounts for nearly 70% of the individual's daily energy expenditure it can be used to guide weight loss programs or for nutritional programs.

The systems must be simple to use, accurate, self-calibrating, fast, and affordable.[34] There has been some discussion on the validity of these portable devices as they often report significantly different results than standard metabolic carts.[45-48]

5.3.2. NASA

In space several regulatory mechanisms in the cardiovascular system are adapted to the microgravity environment. These adaptations adversely results in cardiovascular deconditioning, bone density loss, and muscular atrophy.[49,50] Upon returning to the Earth's gravitation field some degree of orthostatic intolerance has been noted in even short duration flights of only a few hours.[51,52] This cardiovascular instability is even more pronounced during prolonged exposure to microgravity and may only be partially reversible. As space exploration progresses from short to long term duration (months to years) flights, it will become more imperative for both the mental and physical well-being of crew members that effective countermeasures be developed.[53-55]

The health of astronauts is closely monitored before, during, and after space flight through periodic noninvasive stress tests.[56,57] The most commonly measured parameter, aboard the space station is maximum oxygen uptake ($VO_2$ max) because multiple body systems must work together during exercise to facilitate the transport of oxygen to the tissues and meet the increased energy requirements. Consequently, $VO_2$ max helps track cardiovascular deconditioning due to weightlessness and assess the effectiveness of resistive exercises.[58,59]

NASA currently utilizes a random access mass spectrometer (RAMS) system known as the Gas Analyzer System for Metabolic Analysis Physiology (GASMAP) to measure crew aerobic capacity. The GASMAP has the drawback of being of being large and bulky. It requires one 1 x 8 panel unit drawer and two 1 x 4 panel unit drawers and weighs 51 kg total. It also requires significant amount of power (205 watts).

REFERENCES


1. McClave SA, Lowen CC, Kleber MJ, McConnell JW, Jung LY, Goldsmith LJ: Clinical use of the respiratory quotient obtained from indirect calorimetry. Journal of Parenteral and Enteral Nutrition 2003; 27: 21-26

2. Wolff HS: Modern techniques for measuring energy expenditure. Proceedings of the Nutrition Society 1956; 15: 77-80

3. Shephard RJ: A critical examination of the Douglas bag technique. The Journal of Physiology 1955; 127: 515-524

4. Badman ER, Cooks RG: Special feature: Perspective - Miniature mass analyzers. Journal of Mass Spectrometry 2000; 35: 659-671

5. El-Aneed A, Cohen A, Banoub J: Mass Spectrometry, Review of the basics: Electrospray, MALDI, and commonly used mass analyzers. Applied Spectroscopy Reviews 2009; 44: 210-230

6. Palmer PT, Limero TF: Mass spectrometry in the U.S. space program: Past, present, and future. Journal of the American Society for Mass Spectrometry 2001; 12: 656-675

7. Merilainen PT: Metabolic monitor. International Journal of Clinical Monitoring and Computing 1987; 4: 167-178

8. Macfarlane DJ: Automated metabolic gas analysis systems - A review. Sports Medicine 2001; 31: 841-861

9. Hodges LD, Brodie DA, Bromley PD: Validity and reliability of selected commercially available metabolic analyzer systems. Scandinavian Journal of Medicine & Science in Sports 2005; 15: 271-279

10. Saklad M, Sullivan M, Paliotta J, Lipsky M, Brown BR, Jr.: Pneumotachography: A new, low-dead-space, humidity-independent device. Anesthesiology 1979; 51: 149-153

11. Jaffe MB: Infrared measurement of carbon dioxide in the human breath: "Breathe-through" devices from Tyndall to the present day. Anesthesia & Analgesia 2008; 107: 890-904

12. Clark LCJR, Wolf R, Granger D, Taylor Z: Continuous recording of blood oxygen tensions by polarography. Journal Applied Physiology 1953; 6: 189-193

13. Kanwisher J: Polarographic oxygen electrode. Limnology and Oceanography 1959; 4: 210-217

14. Stambouli AB, Traversa E: Solid oxide fuel cells (SOFCs): A review of an environmentally clean and efficient source of energy. Renewable and Sustainable Energy Reviews 2002; 6: 433-455

15. Kovacich RP, Martin NA, Clift MG, Stocks C, Gaskin I, Hobby J: Highly accurate measurement of oxygen using a paramagnetic gas sensor. Measurement Science and Technology 2006: 1579

16. Schmid U, Seidel H, Mueller G, Becker T: Theoretical considerations on the design of a miniaturised paramagnetic oxygen sensor. Sensors and Actuators B: Chemical 2006; 116: 213-220

17. Turner PG, Dugdale A, Young IS, Taylor S: Portable mass spectrometry for measurement of anaesthetic agents and methane in respiratory gases. Veterinary Journal 2008; 177: 36-44

18. Orr J, Brewer, Lara: Oxygen uptake (VO2) measurement system based on novel luminescence-quenching on-airway oxygen sensor. Anesthesiology 2007; A1642

19. Orr J, Brewer, Lara: Clinical evaluation of an on-airway system to measure oxygen uptake. Anesthesiology 2008; A281

20. Orr J, Brewer, Lara: Evaluation in volunteers of a VO2 measurement system based on a novel on-airway oxygen sensor. Anesthesiology 2008; A1689

21. Saltin B: Malleability of the system in overcoming limitations: Functional elements. Journal Experimental Biology 1985; 115: 345-354

22. Bouchard C, Dionne FT, Simoneau J-A, Boulay MR: 2: Genetics of aerobic and anaerobic performances. Exercise and Sport Sciences Reviews 1992; 20: 27-58

23. Bouchard C BM, Simoneau JA, Lortie G, Pérusse L.: Heredity and trainability of aerobic and anaerobic performances. An update. Sports Medicine 1988; 5: 69-73

24. Saltin B, Kristina N, Costill DL, Stein E, Eva J, Birgitta E, Gollnick PD: The nature of the training response; peripheral and central adaptations to one-legged exercise. Acta Physiologica Scandinavica 1976; 96: 289-305

25. Gollnick PD, Armstrong RB, Saubert CWt, Piehl K, Saltin B: Enzyme activity and fiber composition in skeletal muscle of untrained and trained men. Journal Applied Physiology 1972; 33: 312-319

26. Astrand P-OaR, K: The textbook of work physiology: Physiological bases of exercise 3 edition. New York, McGraw-Hill, 1986

27. Standardization of spirometry, 1994 update. American Thoracic Society. American Journal Respiratory Critical Care Medicine 1995; 152: 1107-36

28. Ross RM, Beck KC, Casaburi R, Johnson BD, Marciniuk DD, Wagner PD, Weisman IM: ATS/ACCP statement on cardiopulmonary exercise testing. American Journal Respiratory Critical Care Medicine 2003; 167: 1451-

29. Johnson AT, Scott WH, Lausted CG, Benjamin MB, Coyne KM, Sahota MS, Johnson MM: Effect of respirator inspiratory resistance level on constant load treadmill work performance. American Industrial Hygiene Association Journal 1999; 60: 474-479

30. Johns DP, Ingram CM, Khov S, Rochford PD, Walters EH: Effect of breathing circuit resistance on the measurement of ventilatory function. Thorax 1998; 53:: 944-948

31. Coyne K, Caretti D, Scott W, Johnson A, Koh F: Inspiratory flow rates during hard work when breathing through different respirator inhalation and exhalation resistances. Journal of Occupational and Environmental Hygiene 2006; 3: 490-500

32. Deno NS, Kamon E, Kiser DM: Physiological responses to resistance breathing during short and prolonged exercise. American Industrial Hygiene Association Journal 1981; 42: 616 - 623

33. Page RT: Constant flow orifice meters of low capacity. Industrial & Engineering Chemistry Analytical Edition 1935; 7: 355-358

34. Andre D, Wolf, Donna: Recent advances in free-living physical activity monitoring: A review. Journal Diabetes Scientific Technology 2007; 1: 760-767

35. Keyser D, R., Jeffrey, R. Friedman: Extrapolation and curve-fitting of calibration data for differential pressure flow meters. Journal of Engineering for Gas Turbines and Power 2010; 132: 024501

36. Finnemore EJ, Franzini, Joseph B: Fluid mechanics with engineering applications, 10 edition. Boston, McGraw Hill, 2002

37. Munson BR, Young, Donald F., Okiishi, Theodore H.: Fundamentals of fluid mechanics, 4 edition. New York, John Wiley & Sons, Inc., 2002

38. Measurement of fluid flow by means of pressure differential devices, Part 1: Orifice plates, nozzels, and Venturi tubes inserted in circular cross-section conduits running full. International Organization of Standards, 1991

39. Reader-Harris MJ, Sattary JA: The orifice plate discharge coefficient equation. Flow Measurement and Instrumentation 1990; 1: 67-76

40. Laws EM, Ouazanne AK: Compact installations for differential flowmeters. Flow Measurement and Instrumentation 1994; 5: 79-85

41. Reed SB, Sprange MP: Flowmeter calibrated for any gas in the range of 1 to 500 liters per hour. Industrial & Engineering Chemistry Fundamentals 1968; 7: 651-655

42. Johansen FC: Flow through pipe orifices at low Reynolds numbers. Proceedings of the Royal Society of London. Series A, Containing Papers of a Mathematical and Physical Character 1930; 126: 231-245

43. Weissman C, Sardar A, Kemper M: In vitro evaluation of a compact metabolic measurement instrument. Journal of Parenteral and Enteral Nutrition 1990; 14: 216-221

44. Melendez JA, Veronesi M, Barrera R, Ferri E, Miodownik S: Determination of metabolic monitor errors and precision under clinical conditions. Clinical Nutrition 2001; 20: 547-551

45. Kretsch MJ, Blanton CA, Baer D, Staples R, Horn WF, Keim NL: Measuring energy expenditure with simple low cost tools. Journal of the American Dietetic Association 2004; 104: 13

46. Nieman DC, Trone GA, Austin MD: A new handheld device for measuring resting metabolic rate and oxygen consumption. Journal of the American Dietetic Association 2003; 103: 588-593

47. Kautza BC, Kastello GM, Sothmann MS: Validation of MedGraphics' VO2000 Portable Metabolic Analyzer and a modified pneumotachometer. Medicine & Science in Sports & Exercise 2004; 36: S222

48. Yeo S, Ronis DL, Antonakos CL, Speers M, Murphy S, Hayashi R, Stegman N: Evaluation of a portable metabolic system with sedentary pregnant women. Medicine & Science in Sports & Exercise 2003; 35: S193

49. Nicgossian AE, Charles JB, Bungo MW, Leach-Huntoon CS: Cardiovascular function in space flight. Acta Astronautica 1991; 24: 323-328

50. Aubert AE, Beckers F, Verheyden B: Cardiovascular function and basics of physiology in microgravity. Acta Cardiologica 2005; 60: 129-151

51. Levy MN TJ: Cardiovascular deconditioning of space flight. Physiologist 1983; 26: 297-303

52. Convertino VA: Status of cardiovascular issues related to space flight: Implications for future research directions. Respiratory Physiology & Neurobiology 2009; 169: S34-S37

53. Leblanc A, Rowe R, Schneider V, Evans H, Hedrick T: Regional muscle loss after short duration spaceflight. Aviation Space and Environmental Medicine 1995; 66: 1151-1154

54. West JB: Historical perspectives: Physiology in microgravity. Journal of Applied Physiology 2000; 89: 379-384

55. Macias BR, Groppo ER, Eastlack RK, Watenpaugh DE, Lee SMC, Schneider SM, Boda WL, Smith SM, Cutuk A, Pedowitz RA, Meyer RS, Hargens AR: Space exercise and earth benefits. Current Pharmaceutical Biotechnology 2005; 6: 305-317

56. Greenleaf JE, Bulbulian R, Bernauer EM, Haskell WL, Moore T: Exercise-training protocols for astronauts in microgravity. Journal of Applied Physiology 1989; 67: 2191-2204

57. Levine BD, Lane LD, Gaffney FA, Buckey JC, Blomqvist CG: Maximal exercise performance after adaptation to microgravity. Medicine and Science in Sports and Exercise 1994; 26: S112

58. Convertino VA: Planning strategies for development of effective exercise and nutrition countermeasures for long-duration space flight. Nutrition 2002; 18: 880-888

59. Ferretti G, Capelli C: Maximal O-2 consumption: Effects of gravity withdrawal and resumption. Respiratory Physiology & Neurobiology 2009; 169: S50-S54